[redacted] for ARS meeting,
Prepr[redacted] 14-16, 1962
Ma[redacted]

Goddard

ONBOARD COLLOIDAL PARTICLE GENERATOR FOR ELECTROSTATIC ENGINES

By Carl T. Norgren

Lewis Research Center
National Aeronautics and Space Administration
Cleveland, Ohio

E-1578

ABSTRACT

The colloidal-electrostatic rocket appears useful as an engine for space missions. At the present time full advantage cannot be taken of its potentialities due to unsolved technical problems. One of these problems is the adequate and reliable production of colloidal particles.

A method of colloidal particle generation based on the expansion of a material through a supersonic nozzle has been investigated and is shown to be capable of supplying particles suitable for acceleration in an electrostatic engine. The material is heated in a small vaporizer which supplies a homogeneous vapor to a convergent-divergent two-dimensional nozzle 15.5 cm. long with a rectangular throat 0.273 by 4.48 cm. Flow rate and subsequent particle growth are controlled by regulating temperature, and hence vapor pressure, of the material in the vaporizer.

Particle size was determined theoretically by assuming each collision is a sticking collision after expansion and a correlation of diameter proportional to time was obtained. The experimental particle size determination was obtained by visual inspection of photographs taken in an electron microscope. It is demonstrated that particle size can be controlled from 50 to 500 angstroms and maintain narrow range distributions suitable for engine application. Experimental verification of particle size was determined by collecting a portion of the nozzle exhaust beam

(immediately after the nozzle exit) on a fine grid coated with a silicon dioxide film. The grid was maintained at liquid nitrogen temperature until transferred to the electron microscope. By means of a carefully controlled partial monolayer deposition of material on the sample grid, it was also established that most of the propellant was converted into a useable colloid.

The colloidal generator was incorporated into a small specialized electrostatic engine. A negative corona discharge was used to charge the colloidal particles and Pierce accelerator was used to accelerate these particles. A calculated thrust density of ~~9.34~~ 5.60 $\times 10^{-3}$ Newtons/m^2 at a specific impulse of ~~750~~ 420 seconds was obtained in engine operation.

INTRODUCTION

The use of electrostatic rocket engines as a propulsion system for a variety of satellite and interplanetary space missions appears promising (Refs. 1 and 2). For missions of this type specific impulses from 1,000 to 10,000 sec are required (Ref. 3). A colloidal-particle electrostatic rocket engine in which sub-micron sized particles are charged and then accelerated may be capable of meeting flight requirements. High power efficiency, high propellant utilization, reasonable field strengths, physical and electrical reliability, light weight, and long-duration operation are all required of the electrostatic rocket engine (Ref. 4).

The colloidal-particle engine first of all requires a supply of sub-micron particles which can be charged and accelerated. It is readily shown that extremely high potential differences in the order of 1×10^6 to 1×10^8 volts are required for acceleration of singly-changed micron

sized particles (Ref. 5). If however, particles in the order of 0.001 to 0.01 microns can be utilized, then more realistic accelerating potentials can be used. The generation of these colloidal particles must then satisfy several requirements: first, they must be in the sub-micron range; second, sufficient quantities of particles must be produced to satisfy mission requirements; and third the range and size distribution must be such that relative thrust losses due to exhaust velocity distributions are small (Ref. 6).

The selection of a colloidal particle must be further restricted by practical application. It would be desirable to produce colloidal particles at will with the option of controlling thrust by varying particle size. This implies manufacture "on board" the spacecraft. Several sources of preformed colloids are available (Refs. 7 and 8), but necessitate preparing the colloid in a state suitable for a propellant. This preparation is complicated in that the colloid is usually in some sort of a carrier due to high reaction rates and even after separation the finely divided particles are subject to agglomeration which makes the use of such a preformed material difficult (Ref. 9). On board preparation should be accomplished with a minimum of complexity and a maximum of reliability.

In addition to the application of the colloidal particle engine to short range flights as previously mentioned, there are a number of long range missions for which the colloidal engine could be suited. A colloidal generator capable of providing a large number of heavy particles would enable an electrostatic rocket of large thrust variations to be

used. By proper material selection it would be possible to make radiation losses insignificant. A stepped linear accelerator could be used with this system to obtain the potential difference required to attain a high specific impulse. An analysis of the design of a stepped accelerator is available (Ref. 10); however, an analysis of the mission would be required to determine the actual accelerating potential.

The selection of a system to provide colloidal particles for an electrostatic rocket engine has been the subject of extensive research. Many methods have been and are being considered, such as: prepared particles (Refs. 6, 11, and 12), formation of charged liquid droplets (Refs. 13 through 17), condensation, (Ref. 18), etc. The literature not only contains a number of methods, but also a multitude of theoretical explanations as to the mechanism of particle formation. This report is intended to describe a colloidal generator that delivers particles of relatively narrow size range suitable for electrostatic acceleration.

In considering the design of the colloidal particle generator it has been observed that the expansion of certain materials in a turbine nozzle produced condensation of the materials on the turbine blade (Ref. 19). Analysis of the deposit indicated that the coating was composed of sub-micron particles that had been formed in the exhaust stream. Condensation from a supersaturated vapor, obtained by expansion in a supersonic nozzle, was used for this method of particle generation. In this design a molecular vapor was introduced into a convergent-divergent nozzle having a rectangular throat 0.273 by 4.48 cm. The particle growth

rate was controlled by the number of collisions during adiabatic expansion of the gas in the nozzle. The number of collisions are dependent on the vapor pressure, molecular weight, and dwell time.

An experimental electrostatic rocket engine was assembled employing the colloidal particle generator designed with a means of charging the particles. The charged particles were accelerated in a Pierce type accelerator. The electrostatic engine design was not considered optimum and was used for exploratory purposes only; however, limited data on performance was obtained with this system.

COLLOIDAL PARTICLE ENGINE DESIGN

Colloidal Particle Generator

Condensation from a homogeneous vaporized material in a convergent-divergent nozzle was selected as a means of producing particles. In this system vaporization, nucleation, condensation, agglomeration, and possibly evaporation take place in the order of 1 millisecond; consequantly, very little generalized experimental data is available due to the complexity of the kinetics of the system.

It can be shown that surface energy can be neglected above a critical diameter of 0.02 microns (Ref 20). Since it will be shown that particles under consideration will be less than this diameter, surface energy could play an important role in determining particle size. Other mechanisms could be considered such as discussed in Ref. 21; however, the following simplified treatment was considered:

The surface energy of 1 gram of particles with surface tension σ, and diameter D_p is

$$E = \sigma_p A_p n \tag{1}$$

where

A_p the surface ~~energy~~ area of the particle

E the total energy per gram

ρ the density of material

n the number of particles

Since

$$(n)\left(\frac{\pi}{6} D_p^3\right) = \frac{1}{\rho}$$

and

$$A_p = \pi D_p^2$$

it follows that

$$E = \frac{6\sigma}{\rho D_p} \tag{2}$$

Equation (2) shows that the surface energy is large for small particles. The amount of energy released when two particles a and b of the same diameter form a new particle c is

$$(E_a + E_b) - E_c = \Delta E \tag{3}$$

The volume of the new particle must be equal to the sum of the equal volumes of a and b hence the diameter of the new particle c is

$$D_c = 2^{1/3} D_{a,b}$$

from Eq. (1) for 1 gram of particles

$$\Delta E = (2 - 2^{2/3})E_{a,b}$$

or the fraction of the initial surface energy released is

$$\frac{\Delta E}{2E_{a,b}} = 0.206$$

This energy must be liberated to the surroundings or evaporation will take place.

The rate at which excess energy must be dissipated to the surroundings is determined by the number of inelastic collisions the particle makes. In the model considered, it is assumed that each collision will be with a particle of the same kind because of the absence of air. Assuming that a particle of diameter D_p, will collide with any other particle whose center lies within the distance D_p it can be shown (Ref. 22) that

$$\frac{dN_c}{d\tau} = \frac{4}{3} \pi n_p D_p^2 u_p \tag{4}$$

where

N_c number of collisions per unit time

n_p number of particles per unit volume

u_p average velocity of the particles

τ time

Since it was assumed that after a collision the two particles will result in the formation of a single particle, the volume of the new particle is sum of the volumes of each of the colliding particles. Hence, growth rate can be expressed as:

$$\frac{dV_p}{d\tau} \propto \frac{dN_c}{d\tau} \tag{5}$$

It can be shown that the general equation for growth rate is:

$$D_{p,\tau}^{5/2} - D_{p,0}^{5/2} = k\tau \tag{6}$$

substituting the following in consistent units:

μ velocity of ideal gas molecule = $\sqrt{\frac{3\ RT}{M}}$

M atomic mass unit of particle = $W_p N$

W_p particle weight = $\frac{1}{6}\pi D_p^3 \rho_p$

where

$D_{p,\tau}$ the diameter after a given time τ

$D_{p,o}$ the initial diameter

k $20.56 \times 10^{-12} \frac{(W_t)}{\rho_p}\left(\frac{RT}{\rho_m}\right)^{1/2}$

N Avogadro's number

R gas constant, dyne-cm/(mole)(^{o}K)

T temperature, ^{o}K

W_t weight flow of material, g/sec

ρ_p particle density

τ time

Supercooling of the material was accomplished by adiabatic expansion in a convergent-divergent nozzle designed by the method of characteristics (Ref. 23). From a consideration of particle surface energy the nozzle expansion ratio was determined. The dwell time required was established by the nozzle length which in turn fixed the throat area. A sketch of the nozzle is shown in Fig. 1(a). The nozzle as constructed could be operated over a considerable range since the dwell time could be readily varied. Dwell time is dependent on the acoustical velocity ~~of sound~~ in the medium which in turn is a function of the temperature and molecular

weight of the material. A compromise length of about 15 centimeters corresponding to a residence time of 0.00067 seconds was used. No attempt was made to optimize a nozzle for a given material and particle size at this stage of the investigation.

Particle growth takes place in the nozzle. The nozzle, the vaporizer, and the heaters are referred to as the colloidal-particle generator and are shown in Fig. 1(b) with radiation shields removed. In operation, temperature (recorded by thermocouples) is controlled by radiant heating of the vaporizer and of the nozzle. Three radiation shields are used to prevent heat loss to the surroundings (two over the heating wires and one over the vaporizer end plate).

Operation is usually under choked flow conditions; consequently, the nozzle throat area determines mass flow. Critical ratios for this nozzle are tabulated in table I for a γ of 1.32.

Charging

The method of charging the prepared colloid is not formalized at the present time. Some of the methods that have been considered are: (1) negative charging by electron attachment; (2) positive charging by electron bombardment; (3) positive charging by ion attachment; (4) liquifying material and applying electrostatic potential to break up droplets; (5) static charging by particle rupture; (6) static charging by contact with surfaces having high surface field strengths; (7) field emission of electrons from particles; (8) field emission of ions from particles; and (9) radiation of particles by a radioactive source.

The optimum method has not been established but negative charging by electron attachment was used in this preliminary electrostatic engine. Considering the relatively high pressure levels at the exhaust of the system, controlled electrical breakdown taking the form of a corona discharge was used. Cobine (Ref. 24) gives general equations for discharge currents that can be expected with a corona discharge. From a view point of current, potential gradients, available power supplies, and durability of a 3 mil tungsten wire was used for the corona discharge. A typical operating curve for this emitter is shown in Fig. 2.

Charging efficiency was not considered at this state of system development; however, the charge that can be placed on a colloidal particle is one of the major factors in electrostatic engine design. One of the controlling factors in electrostatic engine design is space charge limited current. Space charge limited current as defined by Childs law is:

$$i_s = \frac{4\sqrt{2}}{9} \epsilon_o \sqrt{\frac{Ze}{m}} \frac{E_A^{3/2}}{L^2} \qquad (6)$$

where

i_s saturation current density, amps/m^2

E_A potential difference, v

L accelerator length, m

The specific impulse of an electrostatic engine can be expressed as,

$$I = \frac{1.414 \sqrt{e/m} \sqrt{E_A}}{g} \qquad (7)$$

I impulse, sec

g gravitational constant

A plot of specific impulse and atomic mass unit for various values of potential difference is shown in Fig. 3 assuming a singly charged particle. A range of specific impulse for the mission considered is also shown. Unless very high accelerating potentials are used a limit must be placed on the particle mass.

In Fig. 4(a) the atomic mass of a particle composed of molecules with an atomic mass of 250 and an assumed density of 5.0 is shown for sub-micron sized particles. For this purpose, particles and molecules were considered spherical. An indication of the number of molecules required to form such a particle is shown in Fig. 4(b). Depending on the material, a particle size above 0.01 micron need not be considered if a limit of 1×10^6 volts is placed on the accelerating potential. A lower limit of 0.001 microns has been selected based on the premise that heavy molecules could more easily be used.

Up to the present time it has been assumed that only one charge could be placed on the particle. If some means could easily be derived to contain the particle until it is limited by field emission (10^9 volts/meter for perfectly spherical negative particles Ref. 25, and 10^{10} volts/meter for perfectly spherical positive particles Ref. 26) then lower accelerating potentials or larger particles could be utilized. It can be shown the minimum radius a spherical particle could have based on Gauss's law is (Ref. 10);

$$r = \left[\frac{Ze}{4\pi\epsilon_o (E_m - E_A)} \right]^{1/2} \tag{8}$$

where

E_m the field strength for field emission, 10^9 - 10^{10} volts/m

E_A the applied field strength

This equation is plotted in Fig. 5 for limiting charge to mass ratios of a particle composed of atomic mass units of 250 and a density of 5.0. A dashed line indicates charge to mass ratios of singly charged particles that fall below the minimum diameter as predicted from charged spheres. The charge in the small diameter case must be attached by some other mechanism, such as associated with positive or negative ions.

From these considerations (maximum charge, accelerating potential, and specific impulse) it is concluded that a charge-to-mass ratio of 10^3 to 10^4 coulombs/kilogram can be considered at the present time, within a particle size range of 0.001 to 0.01 microns.

Accelerators

The accelerator design followed the Pierce boundary conditions with space charge limited flow (Ref. 27). The accelerator aperture is a rectangular slot 0.273 by 7.50 centimeters. The Pierce accelerator electrodes were spaced at 20 millimeters.

It has been shown (Ref. 10) that high field strengths are very desirable in improving thrust per unit area. Since perfectly spherical particles can sustain field strengths of 10^9 to 10^{10} volts/meter, if the accelerator could sustain comparable field strengths then higher impulses with colloidal particles could be attained.

For Childs Law accelerators it has been shown that (Ref. 28):

$$L = 0.664 \times 10^{-6} \left(\frac{\Delta V_A}{\Delta V_{net}} \right) \frac{mI^2}{zeE_A}$$

where

L	accelerator length, m
$\Delta V_A/\Delta V_{net}$	accelerator field strength (ratio), let equal to 1
m	mass
ze	charge
I	impulse
E_A	accelerator field strength

For z equal to 1, the accelerator lengths are shown in Fig. 6 for a range of field strength and for two specific impulse values of 1000 and 10,000 seconds. If a nominal accelerator length of 1 centimeter is assumed to be a practical value for spacings of accurately machined electrodes, it is evident that cesium or mercury accelerators will have field strengths of 10^6 volts/meter only at the higher values of specific impulse; while colloidal particle accelerators with a particle mass of 10^4 a.m.u. would have a field strength of nearly 10^6 volts/meter at a specific impulse of 10,000 seconds.

From the preceding discussion, it is apparent that colloidal particle electrostatic rocket engines may have a definite practical advantage over the contact-ionization and electron-bombardment engines with regard to thrust per unit area. To further emphasize this point, accelerator length vs. field strength is shown in Fig. 7 for a specific impulse of 5000 seconds (which is of current interest for some space missions) (Ref. 28). To take full advantage of the presently attainable field strengths (3×10^6 volts/m), the contact-ionization and electron-bombardment engines would require accelerator electrode spacings of about

1 millimeter, while a colloidal-particle engine with $M = 10^4$ a.m.u. could have electrode spacings of over 5 centimeters. If higher field strengths become practical in the future, the colloidal-particle engine will become even more desirable.

Colloidal Engine

The aforementioned components were incorporated into a colloidal electrostatic engine as shown in Fig. 8(a). The generator was indirectly heated by an a-c nichrome heating unit wound around the vaporizer, and an a-c nichrome wire wound around the nozzle. The entire unit was maintained at zero potential with respect to ground. Three radiation heat shields were used to limit heat flow to the tank walls.

The colloidal particles were negatively charged by a negatively charged corona wire. These particles were then accelerated to ground. A 0.63 centimeter lava plate was used to cover the entire exhaust faceplate. Insulating bolts, lava blocks, and sapphire balls were used to mount the various components to this plate. To prevent reverse flow in the engine an "electron trap" system was installed. This system, shown in Figs. 8(b) and (c), consists of a 0.63 centimeter tube placed around the nozzle exit, and a wire mesh screen placed over the whole area in the vicinity of the exhaust. It was found experimentally that this wire screen was necessary to prevent arcing and to confine the corona. This trap was maintained at a high negative potential.

Colloidal particles entered the charging area with a specific impulse of about 25 seconds from the colloidal generator. The electron and particle densities were such that most of the particles would have an opportunity to collide with an electron before passing through the charging zone.

The first accelerator was maintained at a high negative potential. The corona wire was maintained at a higher negative potential. Due to the corona wire incorporated into the system the accelerator optics were distorted. It was assumed in any calculations that the accelerator spacing was the physical distance between the accelerator plates, and that the charged particles entered the accelerator at zero velocity. The final accelerator plate was maintained at ground potential. A cooled collector was placed downstream of the exhaust.

To facilitate experimental operation, a scale mock-up of the engine was used with a stretched rubber-membrane analog. By observing the path of travel of plastic balls through the system, rough operating potential gradients were established, and minimum impingement on electrodes obtained. The deflection of a rubber analog follows Laplace's equation in two dimensions, which only holds in a charge free region. Since a space charge is present this simplified method cannot hold; however, this procedure can provide a fair approximation.

PROCEDURE

Material Selection

The selection of materials for use in the colloidal generator has been based primarily on physical properties. Up to the present time, only those materials readily available with a narrow boiling range, or those which sublime have been considered. "Boiling" temperatures in the range from one hundred to several hundred ^{o}C at a pressure of 1 millimeter afford the best means of control in the vaporizer without resulting in high radiation heat losses. Limited data have been obtained with three materials; (1) mercuric chloride m.w. 271; (2) aluminum chloride

m.w. 133; and (3) mercurous chloride m.w. 236. Physical properties of these materials are summarized in Table II.

Colloidal particle size evaluation. - All sample runs were obtained in a small bell jar vacuum chamber using a 6 inch diffusion pump. Pressures were maintained usually between 10^{-5} and 10^{-6} mm of mercury.

The material to be used was placed in the vaporizer. The vaporizer and the nozzle were heated independently to a predetermined temperature. The exhaust stream was sampled by placing small sample plates over the nozzle exit.

Two methods were used to initiate propellant flow. First, the material was placed in a small capsule which in turn was placed in the vaporizer. When operating temperature was reached the capsule was opened by an electric pulse. This method was soon discarded during colloidal sampling because the initial burst of propellant and trapped gases would carry relatively large chunks of material to the sampling plate. In the second method, material was placed directly in the vaporizer. The system was evacuated, heat applied, and then the sample was obtained. To prevent material from depositing on the sample plate a cooled copper plate was placed between the sample and the nozzle. This plate was removed for a short time during actual sampling. After the sample was taken this plate prevented the collecting surface from seeing any warm body and thus reduced side effects that would influence particle size. A sketch of this sampling system is shown in Fig. 9(a).

The copper plate served an additional purpose in that the material would deposit out on the plate since it was usually cooled by liquid

nitrogen. This deposit served to indicate how material left the nozzle. A macrograph of a deposit obtained on the copper plate is shown in Fig. 9(b). The cross-sectional deposit is relatively uniform over the nozzle width. The deposit that was exposed to the nozzle has melted and formed smooth globs on the surface since the the deposit was so thick that heat could not be readily transferred to the heat sink. This type of deposit is typical of that obtained along the length of the slot.

The sample plates were viewed in an electron microscope to indicate particle size. Due to the momentum of the particles many collecting films could not withstand the particle impingement and shattered. The sample plates that seemed to give the best results were made on a 200 mesh nickel grid. The grid was approximately 3 millimeters in diameter with a silicon dioxide film deposited on the surface.

Several methods were used to suspend the sample plate during sampling, such as, placement on parallel copper wires, using glucose to cement the sample plate to a wire, or using one of the hard waxes. In any case, the useable sampling surface was not allowed to contact any material or surface except the exhaust stream of the nozzle, because the sample plate contaminated easily, and the silicon dioxide film was fragile.

Engine operation. - After the samples were obtained, the nozzle of the colloidal-particle generator was incorporated into the electrostatic engine as shown in Fig. 8. The power supplies were connected as shown in Fig. 10. The power supply voltages are low when considered for colloidal-electrostatic engine operation; however, these supplies were readily available and served for a preliminary test of the engine. After

the colloidal stream was stabilized the power supplies were turned on and the corona discharge operated. Potentials were selected based on the rubber-membrane analog. The charged particles were collected in a cooled chamber. All currents were measured with micro-ammeters.

RESULTS AND DISCUSSION

As previously mentioned, particle sizes from 0.001 to 0.01 microns are desired from a mission consideration, and the colloidal particle generator was designed to provide the opportunity for this growth from a vapor phase. Nozzle performance was based on the visual inspection of photographs obtained from sample plates located at the nozzle exhaust. Since the particles are in the sub-micron size range, these sample plates were viewed in the electron microscope. To obtain reliable photographs with a minimum of side effects (such as melting or aggregation), the beam power intensity was kept low.

Since the nozzle performance was based on results obtained from the electron microscope, it is necessary to consider the interpretation of the image. In such applications as the flashing of a material, or the expansion of a material through a nozzle into high vacuum, the vaporized material arrives on the collecting film as atoms or molecules. The mean free path in such applications is usually great compared to the distance between the source and the collecting film, hence, the particles that are "viewed" are formed by growth on the collector. In fact, one investigator is conducting a program by using this observed growth for particle generation (Ref. 29). In the system described in this report however, the particles are formed by collision in the gas phase (Ref. 19).

Since it had been shown that particle residence times can be as low as 40 microseconds for condensation to occur in a supersonic wind tunnel (Ref. 30), the nozzle should be well within any critical time period. It has further been shown that metallic particles can be formed in an inert gas by atomic condensation (Ref. 31). In Ref. 31, many experimental micrographs are shown to indicate the effect of pressure on the formation of particles. For this reported data a known amount of material was vaporized and the presence of an inert helium atmosphere was used to control collision rate.

COLLOIDAL GENERATOR

Three materials, that have been used in the colloidal-particle generator are presented in the following discussion.

Mercuric chloride. - Micrographs of mercuric chloride are shown in Fig. 11. In this figure, the film has been shadowed to bring out particle detail. The supporting film is clearly shown as a finely broken mosaic pattern (Fig. 11(a)). This pattern is characteristic of that formed by atoms on a surface; since the collecting film is formed in a high vacuum this is the pattern that would be expected, and accounts for the background pattern viewed in this micrograph.

The particles which are formed are of the filament and clumped varieties. The particles appear to form a continuous aggregate probably due to the migration of molecules on the surface, since two degrees of freedom are still present and the system favors the reduction of surface energy. The sample plates were not cooled, except by conduction to the pump housing; some vaporization or condensation could have taken place as a result during exposure to the exhaust stream.

The particle size distribution is shown in Fig. 12. The number of particles within a given area were counted and their size noted, this number was then averaged on the basis of a hundred typical particles. By selecting a given size grid all particles within a given diameter range were counted. This diameter range was then used to normalize the particle distribution. The actual distribution factor was defined as follows:

$$\text{Distribution Factor} = \frac{\frac{\Delta D}{n_p} \times 100}{\Delta D}$$

where

ΔD the maximum particle diameter - the minimum particle diameter

n_p the number of particles in the ΔD region

The distribution curves are an indication of approximate particle size. The particle size was varied by temperature control.

The calculated particle size (Eq. (6)) is shown in Fig. 13 for two values of k bracketing the test range. This simplified correlation appears to be capable of predicting the particle size from a given set of operating conditions.

Aluminum chloride. - In Fig. 14, a micrograph of aluminum chloride and a particle size distribution is shown. The sample was obtained with only conduction cooling to the vacuum casing, and the collecting film was a plastic material. An average particle diameter of 0.005 microns was obtained. It was necessary, however, to keep the sample dry due to affinity for moisture. The particles were relatively easy to handle and the material was not particularly poisonous. This material was used to operate the electrostatic part of the engine.

Mercurous chloride. - In Fig. 15, several micrographs are shown. In these runs extra care was taken to keep the sample plate cool. Liquid nitrogen (ℓN_2) was used to cool a copper screen basket in which the sampling plates were mounted. The actual copper mounting wires were connected directly to a ℓN_2 coil. The sample plate was shielded in all directions from radiation and the copper plate which covered the generator exit was also ℓN_2 cooled. Samples for two similar runs are shown in Figs. 15(a) and (b). In these photographs mercurous chloride is viewed on a layer of mercurous chloride particles since multilayers of material were deposited on the silicon dioxide film. When the particle are on top of a similar substance the outer molecules tend to fuse onto the underneath layer rather than migrate as shown in preceeding examples. Liquid nitrogen was used until after the sample plates were brought up to atmospheric pressure. The slides were then viewed in the electron microscope.

The particle size distribution is shown in Fig. 16. These particles may be somewhat large for propulsion applications but this operating condition was selected because of the ease in controlling variables and the fact that the vaporizer conditions were in the viscous flow region. The particles were reproduced under four separate runs at a boiler temperature of 488° K. At one of the check points, several additional sample plates were weighed and installed. The increase in weight was taken as an experimental calibration of the flow rate of the vaporizer. A comparison of the actual flow rate and the calculated flow rate for a range of viscous to free molecular flow is shown in Table III for three vaporizer temperatures.

Colloidal-Generator Efficiency

The colloidal-generator efficiency was defined as the fraction of the total material that went into colloidal particle formation. Rather than introduce a whole new set of unknowns such as would be required to completely charge the exhaust products and then measure charge-to-mass ratios, it was decided to try to measure colloidal production by means of the electron microscope.

The electron microscope is capable of a resolution to 0.0015 microns. Most atoms and many molecules have a diameter of around 0.0004 microns. If most of the material could be accounted for in the form of particles then it was assumed that this was the generator efficiency. However, as previously mentioned, atoms depositing on a surface will aggregate to form "visible" particles. To limit this unwanted side effect, a sample was obtained with mercurous chloride with maximum precaution to keep the sample cold, to reduce surface diffusion and subsequent agglomeration. The experimental nozzle flow rate was used, and the sample plate exposed to the stream only long enough to permit a mono-colloidal layer equivalent to 70 percent coverage. The sample plate was then brought up to atmospheric pressure and allowed to come to equilibrium room temperature.

Single molecules have a very high surface energy and tend to evaporate or rebound readily. Since all parts were cooled by liquid nitrogen it was assumed that the vapor pressure of the material, in the vicinity of the sample plate would be low due to cold surfaces. This in turn would prevent particle growth after deposition due to attachment by stray molecules. When the sample was allowed to come to equilibrium room

temperature and room pressure any molecules on the sampling surface would escape into the atmosphere and chances of colliding with the already formed particle would be remote. The particle itself would probably be in a stable state since it has been shown that surface effects are diminished above a critical size (Ref. 20).

The sample plate was then viewed in the electron microscope. In the presence of the electron beam the particles were observed to migrate forming a filament network. This filament network of particles was extremely hard to define due to no contrast. To evaluate the deposit all traces of material were covered with a opaque line as shown in Fig. 17. It was assumed that the depth of particles was the same as the diameter of the particle. The light transmission was then integrated over the film area. From these observations it was calculated that at least 70 percent of the deposited material was accounted for in the form of colloidal particles.

One alternate method of determining particle formation was attempted, but no quantitative results were obtained. During the lN_2 cooled sampling phase of the program, it was observed that mercurous chloride deposited readily on the cold surfaces. An attempt was made to cool a wire screen and collect the amount of material that passed through the screen. By operating the system with different sized particles (controlled by vaporizer temperature) the amount of material which could be collected before plugging of the screen occurred, would be an indication of particle size. Large particles would stick to the wire screen and soon plug up the opening, whereas, a large number of very small particles would pass through before plugging would occur.

The system was operated at a condition where free molecular flow existed in the vaporizer. The system was operated for a considerable length of time and a large amount of material was passed through the screen with no visible effect of blockage. At another condition where large particle size was expected, the screen plugged within a matter of minutes and only a very small quantity of material passed through the screen.

An analysis of the system, assuming each collision a sticking collision, was shown to predict the trend of the results observed; however, on an absolute basis the quantity of material collected did not correspond with that predicted. The amount of material that passed was too high. This could be explained by assuming each collision was not a sticking collision and that the heat lost by each sticking collision heated the immediate area so that no sticking could occur for a short time. This sidelight is included to further show that particle size can be controlled in the nozzle and that several different techniques can be used to point this out.

Colloidal-Electrostatic Engine Performance

The colloidal-particle generator was incorporated into an electrostatic engine configuration as previously shown in Fig. 8. This engine was used primarily to check components and was not necessarily considered as a practical design. A curve showing a typical space charge limited flow current for this engine is shown in Fig. 18; however, the accelerator was actually operated at less than space charge limited flow. For all calculations it was assumed that the particles were

singly charged. At this point, no instrumentation to permit evaluation of the charge-to-mass distribution in the exhaust stream was used. Data obtained with this configuration is tabulated in Table IV.

It has been shown that a corona discharge could transfer almost 100 percent of its charge to a gaseous stream (Ref. 32). In this configuration it was decided to use the electrons from the corona discharge since the electron energy can be kept low, thus preventing fragmentation of the particle. In Fig. 19 the collector current is shown with a negatively charged colloid for a given corona discharge current. A corona charging efficiency, n_c of 50 to 70 percent was obtained for this configuration. This efficiency is defined as

$$n_c = \frac{i_c + i_{i_g}}{i_t}$$

where

n_c corona efficiency

i_c collector current

i_{i_g} impingement current on ground accelerator

i_t total corona current

It has been assumed that impingement on the first accelerator plate was probably due to stray electrons and could not be considered as transported by the colloidal beam. Since the collector and the last accelerator plate are at ground potential it would be possible for stray electrons to be metered as beam current. This is probably not the case since a strong magnetic B field was placed perpendicular to the E field and no drop in current at the collector was noted. If free electrons had

been present they would have been deflected away from the collector plate because of their light mass, while the charged colloidal particles would continue without appreciable deflection. Since only minor focusing of the corona discharge was attempted at this stage, the efficiencies obtained imply that a relatively high percentage of electron attachment occurred.

The operation of the corona discharge was subject to a number of problems. The wire size for a given set of operating conditions was critical. This is one of the variables that can be used to control corona discharge. Depending on the power supplies available the potential gradient can be controlled by wire diameter. If the wire is too small, a spark will initiate and tend to burn out the wire; whereas, if the wire is to large no discharge can be maintained. Under actual operating conditions it was observed that a controlled discharge could be maintained with a negative d-c voltage on the wire; whereas, a positive discharge could be stabilized only at a condition where the system was at a high pressure. The pressure required for stabilization of the negative corona was such that the apparent nozzle exhaust conditions provided the required environment.

As previously mentioned, the operation of the engine served only to determine if the method of colloidal particle generation could be adapted to an electrostatic engine configuration; consequently, performance and operating efficiencies were considered secondary at this stage. Initial operation was limited due to placement of high voltage leads. Also the metering system, in particular the microameters, would

readily burn out if an arc propagated. Many of these problems were easily remedied and operation up to 35 kilovolts was possible.

An attempt was made to calculate the overall operating efficiency of this electrostatic rocket engine configuration. This efficiency was determined as follows:

$$n_e = \frac{P_b}{P_c + P_A + P_i + P_{rad}} n_u$$

where

n_e engine efficiency

P_b beam power

P_c corona power required to produce electrons

P_i power lost by impingement

P_A accelerator power losses

P_{rad} radiation losses

n_u propellant utilization

The beam power was determined by the measured collector current using the potential difference between the corona wire and the collector. The corona power was determined from the corona voltage and current readings. Impingement currents were converted to power assuming corona voltage. Accelerator power losses were determined from voltage and current measurements, when applicable. The radiation power losses were determined from the voltage and current measurements necessary to maintain the boiler and the nozzle at a given temperature level.

The propellant utilization is a calculated value based on the estimated flow of aluminum chloride through the nozzle. The estimate of total flow

The mass flow of aluminum chloride through the nozzle was estimated using the experimental flow rate data for mercurous chloride (Table III). Assuming singly charged particles and the same distribution curve as for uncharged particles the mass flow rate of charged particles was then estimated from the collector current. The ratio of these two mass flows is taken as the propellant utilization efficiency. A propellant utilization efficiency of 56 percent was calculated for a collector current of 75 microamperes.

The calculated engine efficiency for this condition is 30 percent. This calculation is subject to a number of limitations. In addition to the assumptions mentioned above, the actual particle size distribution might not precisely correspond to that in the limited sample taken. The efficiency of this engine may have been limited by electron density which would be relatively easy to increase.

Another factor of interest in engine performance is the thrust per unit area. The thrust per unit area (T/A) is defined as::

$$T/A = MgI$$

where

M total mass flow per unit area at nozzle exit, $kg/m^2/sec = \dot{m}/A$

g gravitational constant 9.8 m/sec/sec

I effective specific impulse, sec

Using aluminum chloride as a propellant and an accelerating potential of 35,000 volts an effective specific impulse of 420 seconds was calculated for a propellant utilization efficiency of 56 percent. At this

condition the thrust per unit area is ~~9.34~~ 5.60 $\times 10^{-3}$ Newtons/m^2, assuming that each particle is singly charged.

Previously, a number of advantages of the colloidal electrostatic rocket have been mentioned. At this point one additional advantage might be considered, radiation loss. In this particular configuration a radiation loss corresponding to 1.23 watts was obtained, no part was hotter than 150° C and the vaporizer itself was maintained between 100° and 125° C. Therefore, radiation losses can be greatly diminished using this approach. By the proper selection of materials it would be possible to operate at still lower temperatures. Thus, an engine of this type can bypass the complicated shielding problems that would arise if high temperatures were used.

CONCLUSIONS

The colloidal-particle electrostatic engine is a potentially high thrust space engine capable of fulfilling many mission requirements. One of the requirements for successful operation of the engine is that a copious quantity of suitable particles be available. This report has described a method of colloidal particle generation that is adaptable to space flight.

The expansion of a material through a supersonic nozzle has been shown to be capable of supplying colloidal particles. Condensation and particle growth take place in the gas phase and are controlled by the state of the material in the vaporizer. Particle sizes are controlled from 50 to 500 Angstroms.

From inspection of electron microscope photographic images it was determined that at least 70 percent of the material was converted to a useable colloid.

A small electrostatic engine was built incorporating the colloidal particle generator. This engine was operated at a calculated thrust per unit area of ~~9.34~~ 5.60 $\times 10^{-3}$ Newtons/m^2 at a specific impulse of ~~150~~ 420 seconds.

REFERENCES

1. Stuhlinger, E.: Possibilities of Electrical Space Ship Propulsion. Extract from Proc. Fifth Int. Astronautics Cong., 1959, pp. 100-109.

2. Moeckel, W. E.: Propulsion Methods in Astronautics. Int. Ser. on Aero. Sci. and Space Flight, Vol. 2, Pergamon Press, 1959.

3. Mickelsen, W. R.: Electric Propulsion for Space Flight. Aero/Space Engineering, November 1960.

4. Mickelsen, William R.: Comparative Performance of Electrostatic Rocket Engines. 30th Annual Meeting of the Institute of Aero/Space Sciences, New York, January 1962.

5. Boden, R. H.: The Ion Rocket Engine. Rocketdyne Report R-645 (AFOSR TN 57-573), August 26, 1957.

6. Wiech, Raymond E., Jr.: Heavy Particle Propulsion Research. Thiokol, Reaction Motors Division Report RMD-1155-S2 (AFOSR-TR 60-48).

7. Ultrafine AL Bids for Markets: Chemical and Engineering News, Vol. 37, Jan. 19, 1959, p. 53.

8. Dow Chemical polystyrene Latex No. 580.

9. Weiser, H. B.: Colloid Chemistry. Second Ed., John Wiley & Sons, Inc., 1950.

10. Langmuir, D. B., and Cooper, R. B.: Thrust Multiplication by Successive Acceleration in Electrostatic Ion Propulsion Systems. ARS Paper No. 929-59, Nov. 1959.

11. Schultz, R. O., and Wiech, R. E., Jr.: Electrical Propulsion with Colloidal Materials. AGARD Comb. and Prop. Panel Tech. Mtg. on Advanced Propulsion Techniques, Pasadena, California, August 24-28, 1960.

12. Shelton, H., Hendricks, C. D., Jr., and Wuerker, R. F.: Electrostatic Acceleration of Micro-Particles to Hypervelocities. Ramo-Wooldridge AFO 4(647)-127, August 10, 1959.

13. Schultz, R. D., and Branson, L. K.: Charged-Colloid Propulsion System. Aerojet General Report 1728.

14. Edmonson, R. B., Kretschmer, C. B., and Becker, L. B.: Charged-Colloid Propulsion System. Aerojet General Report 0290-01-1, AFC 49(638)-656.

15. Cox, A. L., Stevens, M. R., and Kazanjian, A. R.: First Quarterly Report on Propellants for Electrical Propulsion Engines of the Contact or Bombardment Ion Type. Rocketdyne Report R-2513-2, AFC 33(616)-7063.

16. Krohn, V. E.: Liquid Metal Droplets for Heavy Particle Propulsion. Thompson-Ramo-Wooldridge, ARS, November 3-4, 1960.

17. Gignoux, D., Einbinder, H., and Anton, H.: Nozzle for Colloidal Propulsion, Analytical Investigation. Report 19, Cosmic, Inc., Contract NASr-45, August 1961.

18. Sinclair, D., and La Mer, Victor K.: Chemical Reviews 44, Light Scattering as a Measure of Particle Size in Aerosols - The Production of Monodisperse Aerosols, 1949, pp. 245-267.

19. Setze, Paul C.: A Study of Liquid Boric Oxide Particle Growth Rates in a Gas Stream from a Simulated Jet Engine Combustor. NACA RM E55I20a, 1955.

20. Rodebush, W. H.: Nuclei in Evaporation and Condensation. Chem. Rev., vol. 44, no. 2, Apr. 1949, pp. 269-276.

21. Courtney, Welby G.: Recent Advances in Condensation and Evaporation. Texaco Experiment, Inc., ARS Journal, June 1961.

22. Loeb, Leonard B.: The Kinetic Theory of Gases. Second Ed., McGraw-Hill Book Co., Inc., 1957.

23. Liepmann, H. W., and Roshko, A.: Elements of Gasdynamics. John Wiley & Sons, Inc., 1957.

24. Cobine, James D.: Gaseous Conductors. Dover, 1941.

25. Dyke, W. P., Trolan, J. K., Martin, E. E., and Barbour, J. P.: The Field Emission Initiated Vacuum Arc. 1. Experiments on Arc Initiation. Phys. Rev., 91, Sept. 1953, p. 1054.

26. Muller, E. W.: Field Desorption. Phys. Rev., Vol. 102, 1956, p. 618.

27. Pierce, J. R.: Theory and Design of Electron Beams. Second Ed., D. VanNostrand Co., 1954.

28. Mickelsen, William R.: An Introduction to Electrostatic Rocket Engines. Lectures Delivered at NASA Lewis Laboratory.

29. Research on the Acceleration of Heavy Particles. Thiokol Chemical Corporation Reaction Motors Division. RMD 2049, AFOSR Contract AF 49(638)-924.

30. Kantrowitz, A.: Nucleation in Very Rapid Vapor Expansions. J. Chem. Phys., Vol. 19, 1951, p. 1097.

31. Till, Paul H., and Turkevich, John: Metallic Smokes. An Electron Microscope Examination of Aerosols Produced by Evaporation of Metals in Helium. NYO-3435.

32. Whitly, K. T., McFarland, A. P., and Lundgren, D. A.: Generator for Producing High Concentrations of Small Ions. University of Minnesota Technical Report 12, Dept. of Mech. Eng., USPHS Grant S-23.

TABLE I. - CRITICAL RATIOS FOR COLLOIDAL PARTICLE NOZZLE

	~~Total~~ Throat	Exhaust
Temperature/Temperature$_{total}$	0.8621	0.6121
Pressure/Pressure$_{total}$	.5421	.1321
Density/Density$_{total}$	.6289	.2157
Velocity/Speed of sound$_{total}$	.9285	1.5570
Area/Area at speed of sound	1.0000	1.7384
Typical residence time 0.00067 seconds.		

TABLE II. - PHYSICAL PROPERTIES OF SEVERAL MATERIALS

Material	$HgCl_2$	$AlCl_3$	HgCl
Molecular weight	271.5	133	236
Temp. °K, for a vapor pres. of			
760 mm	577	453.3	656.7
76 mm	501	421.2	573
7.6 mm	447	393.6	509
.76 mm	404	369.9	461
0.076 mm	369	349.9	420
Density, g/cc	5.44	2.44	7.55
Heat of formation kg calories	53.4	166.8	31.3

TABLE III. - COMPARISON OF CALCULATED AND EXPERIMENTAL FLOW RATES FOR MERCUROUS CHLORIDE

Temperature, °K	Wt flow gm/sec viscous flow	Wt flow gm/sec free mole flow	Wt flow gm/sec experimental
360	7.44×10^{-3}	9.3×10^{-5}	1.82×10^{-5}
400	5.78×10^{-3}	$.71 \times 10^{-4}$	1.05×10^{-4}
488	1.65×10^{-1}	2.45×10^{-3}	2.86×10^{-1}

TABLE IV. - DATA OBTAINED AT TWO OPERATING CONDITIONS

[3-mil corona wire.]

Trap potential, 5 kv							
Corona		Collector at ground potential current, i_c, μamps	Impingement current engine, i_e, μamps	Impingement on accelerator at ground potential current, i_{ig}, μamps	First accelerator current at ~5.0 kv potential, i_{ia}, μamps	Trap current, i, μamps	Corona efficiency, n_c
Potential, kv	Current, i_t, μamps						
13	3	2	1	0		0	67
14	4	2.5	0	0		0	62
15	5	2.0	0	1		0	60
16	10	5.0	+	+		0	50
16.5	24	6	4	5		+	46
17	40	15	4	10		0	63
Trap potential, 10 kv							
12	3	0	1	0	0	1	0
13.1	10	4	2	0.5	0	1	45
14	26	10	6	4	-4	7	54
14.8	40	17	10	6	-4	12	58
15	70	28	10	15	-8	28	62
15.2	100	50	12	25	-12	40	75

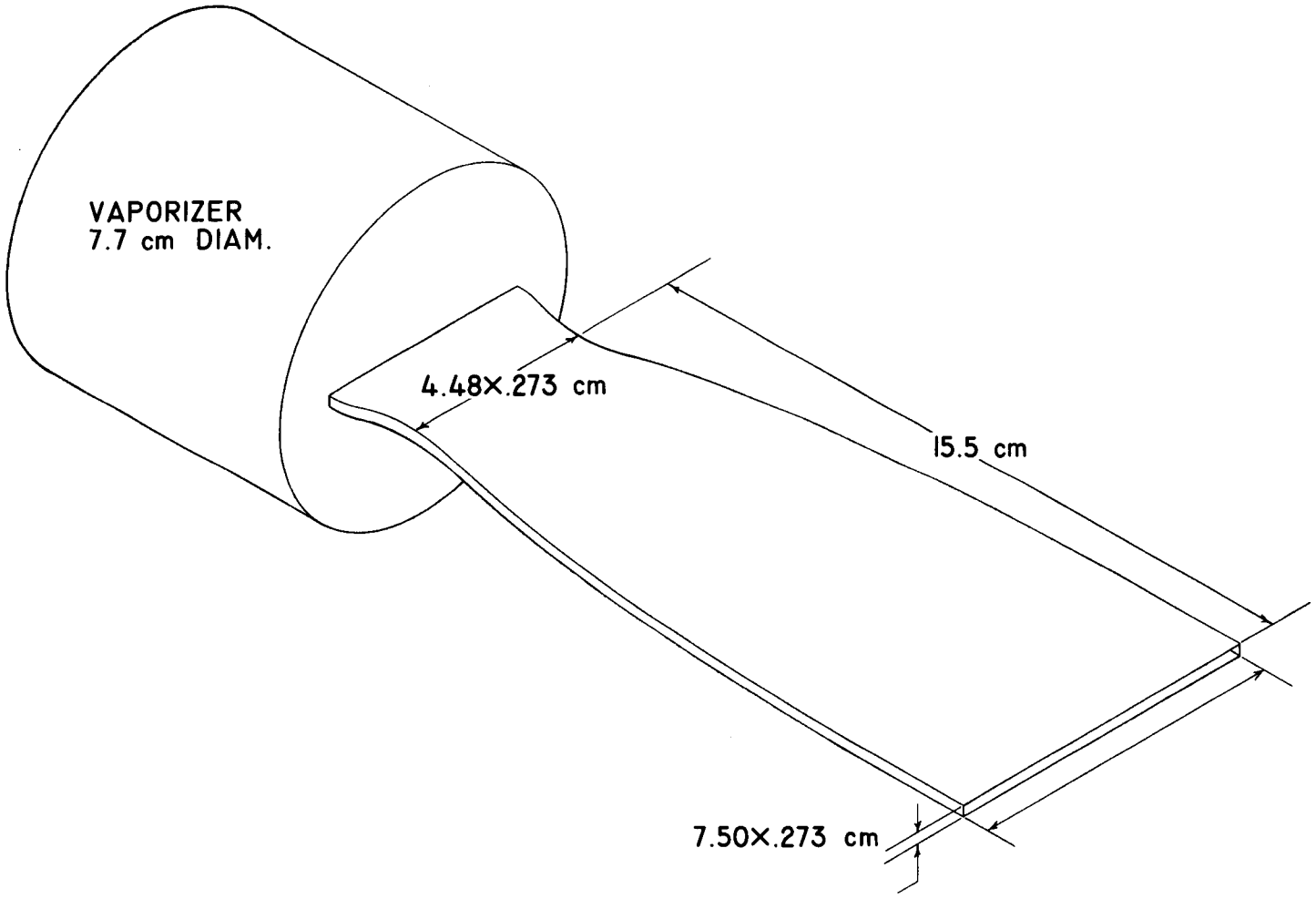

(a) Cross-section colloidal-particle nozzle.

Figure 1. - Colloidal-particle generator.

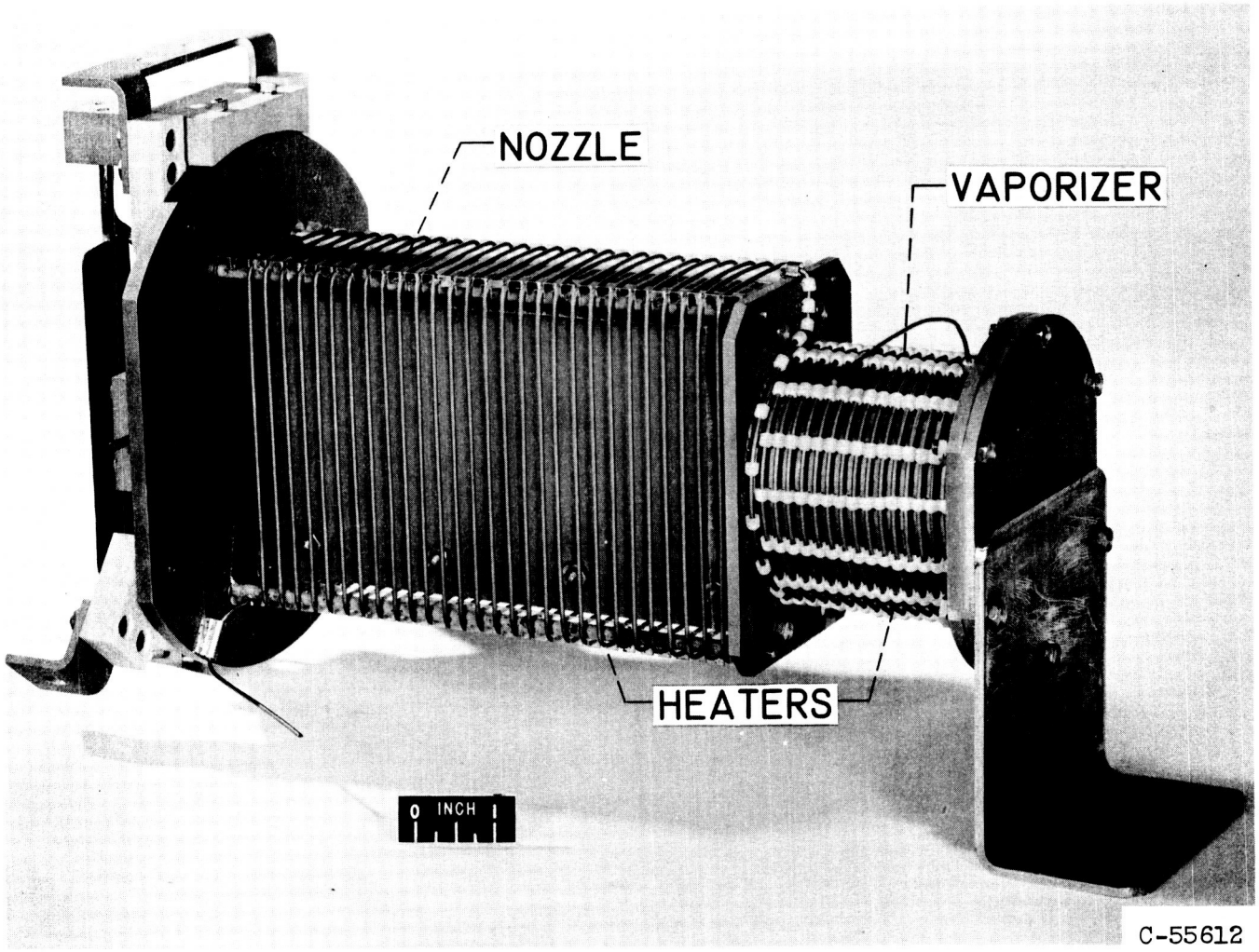

(b) Assembly of nozzle, vaporizer, and heaters.

Figure 1. - Colloidal-particle generator.

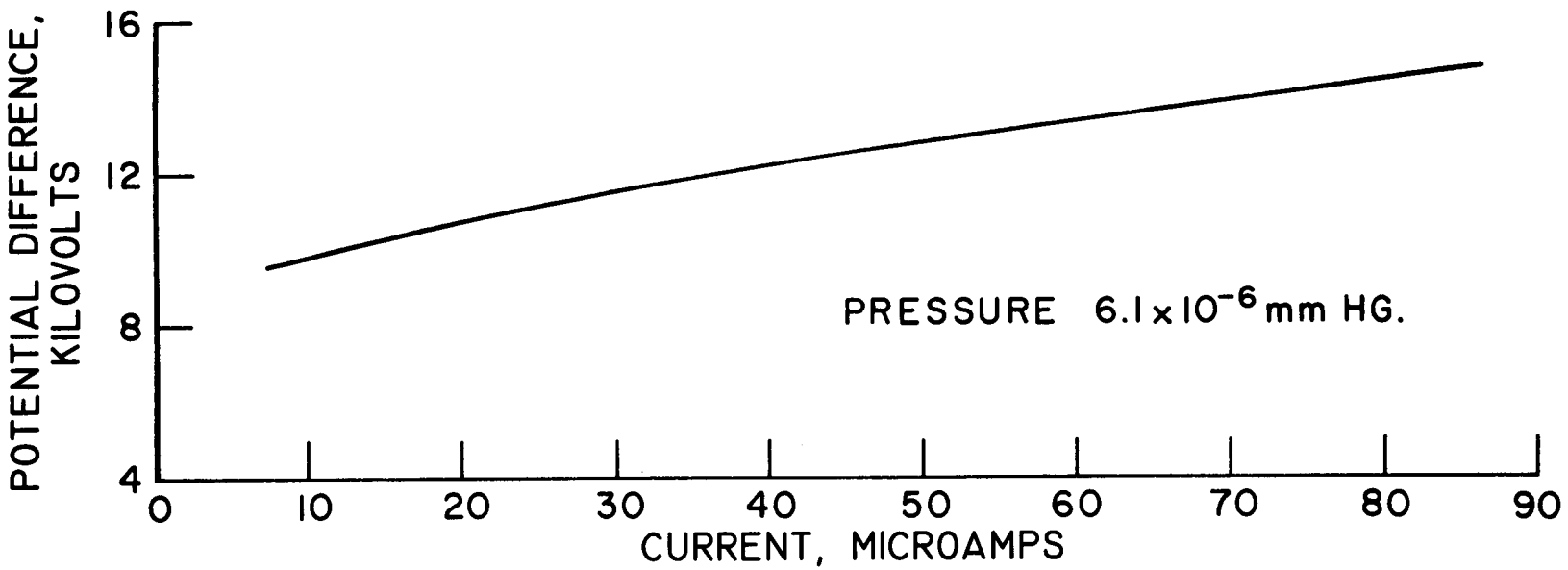

Figure 2. - Typical corona emitter current for a 3 mil wire mounted in the test assembly.

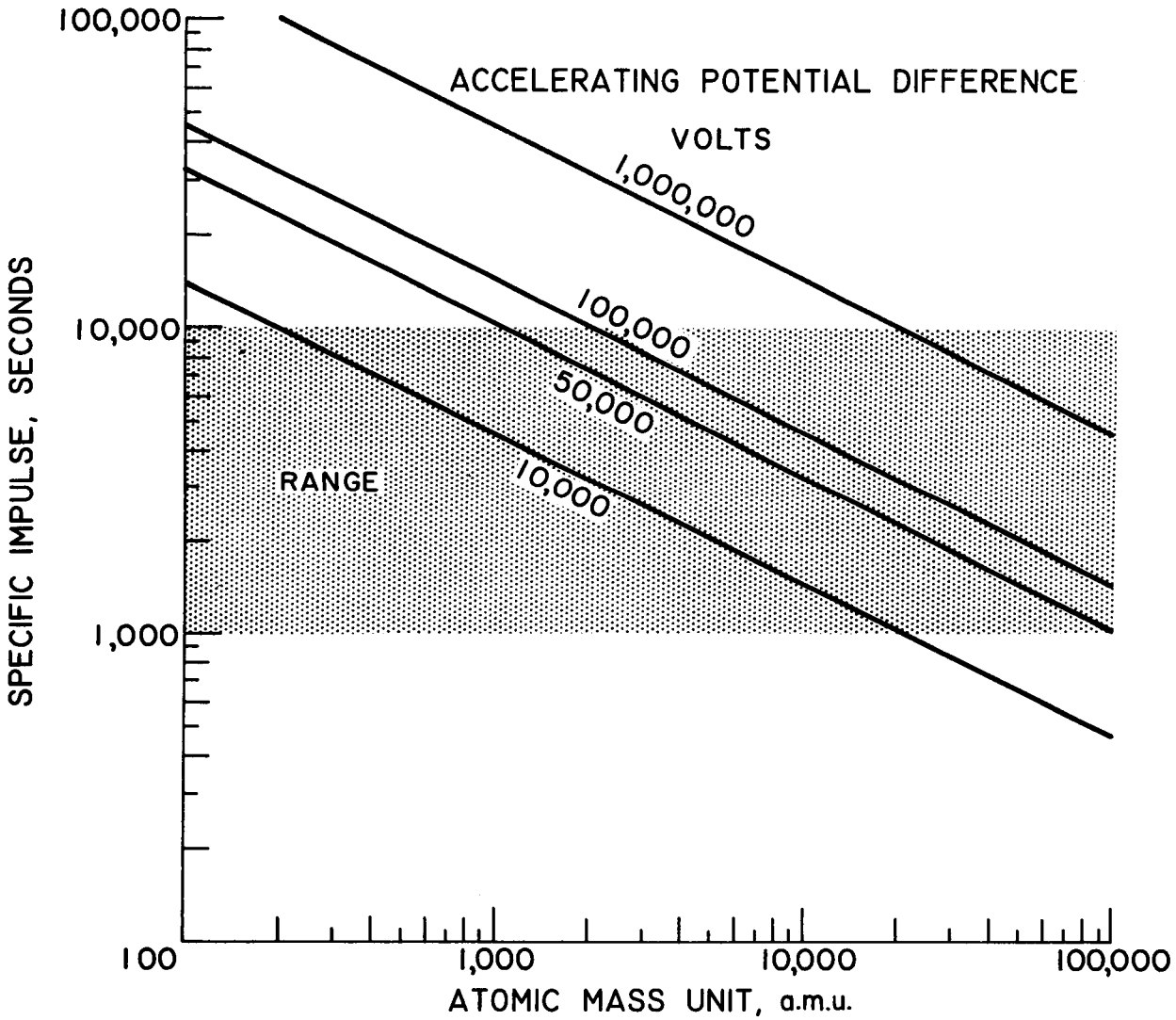

Figure 3. - Specific impulse for a given atomic mass unit.

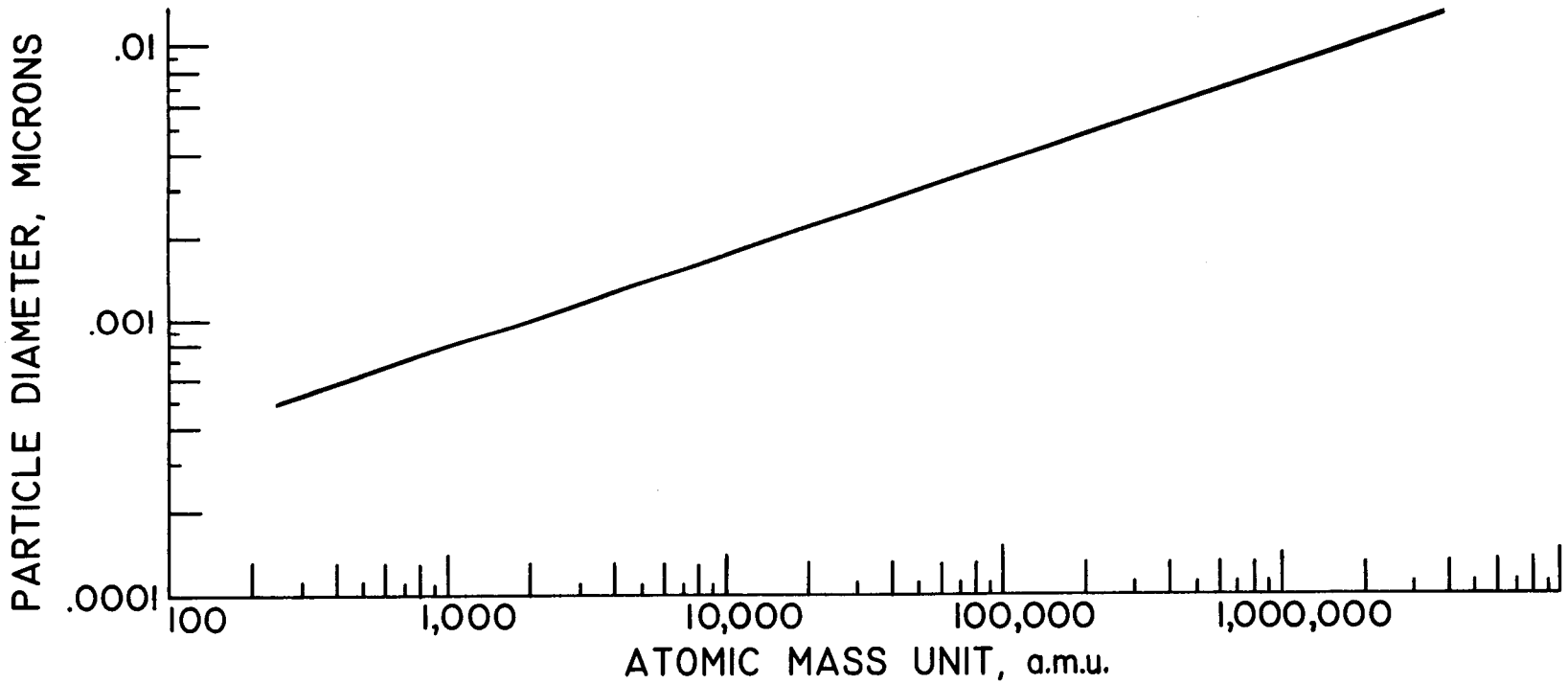

(a) A.M.U. of total particle.

Figure 4. - Conversion of particle diameter for a 250 M.W. molecule.

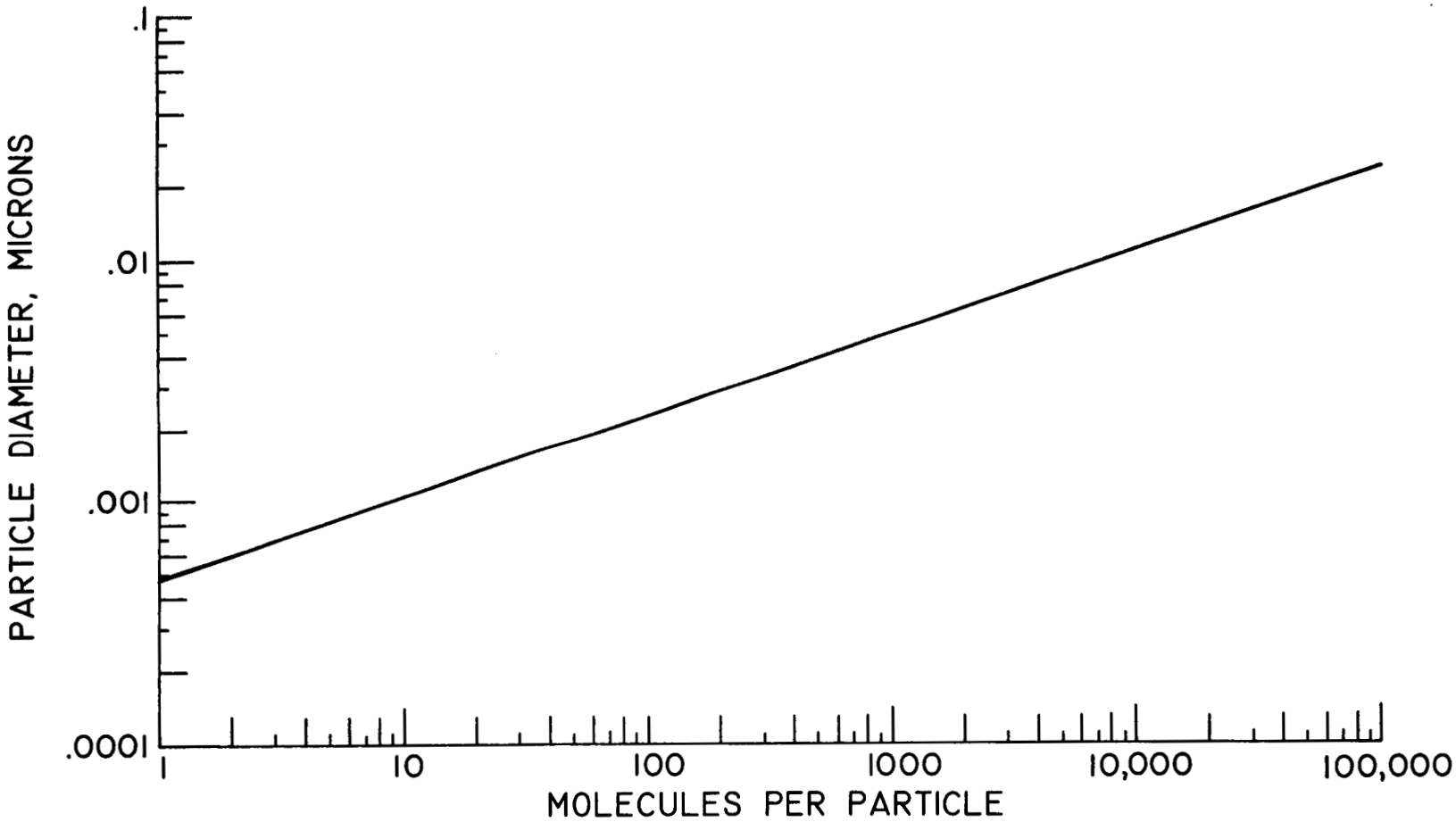

(b) Number of molecules.

Figure 4.- Concluded. Conversion of particle diameter for a 250 M.W. molecule.

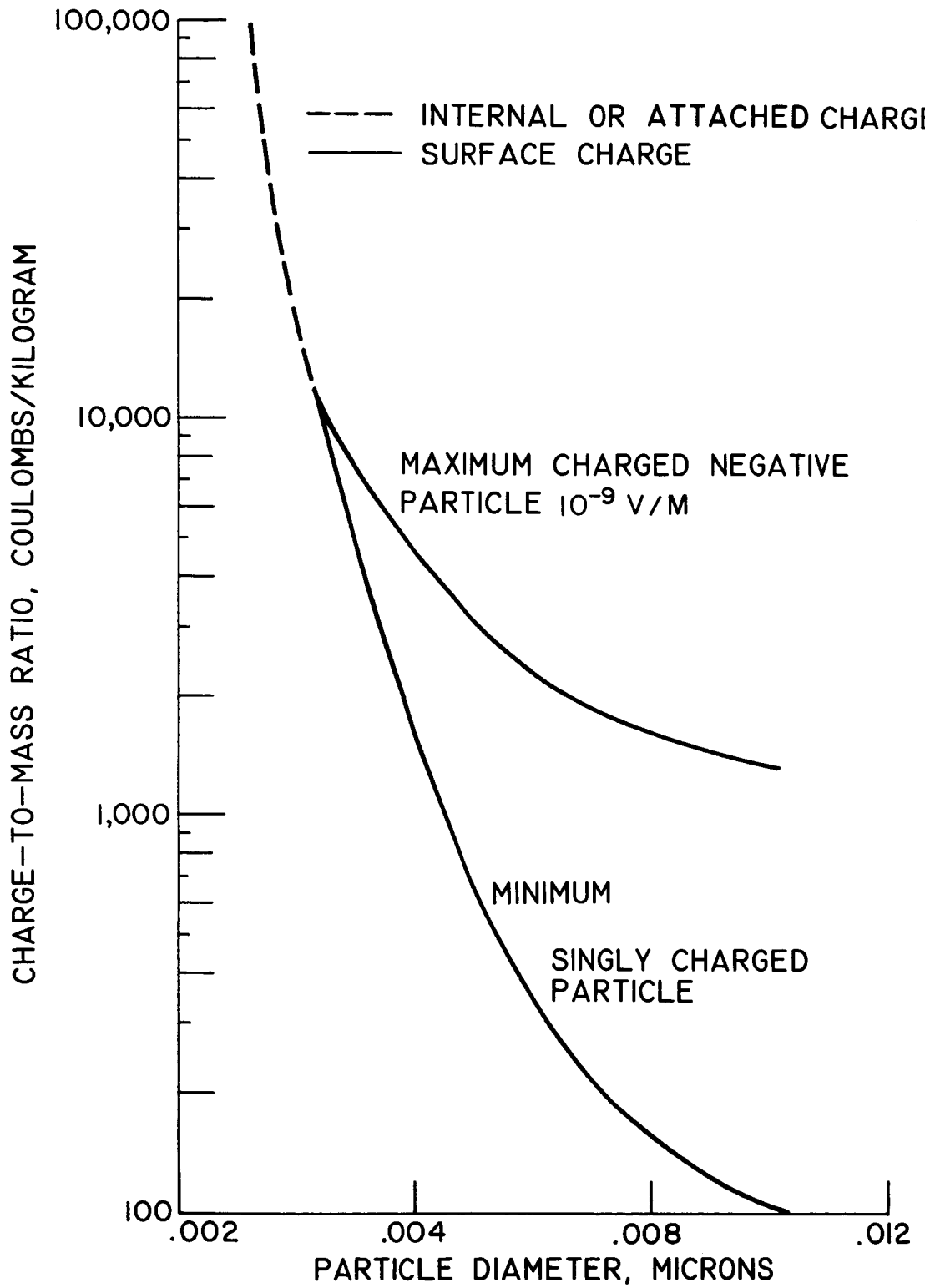

Figure 5. - Charge-to-mass ratio limits.

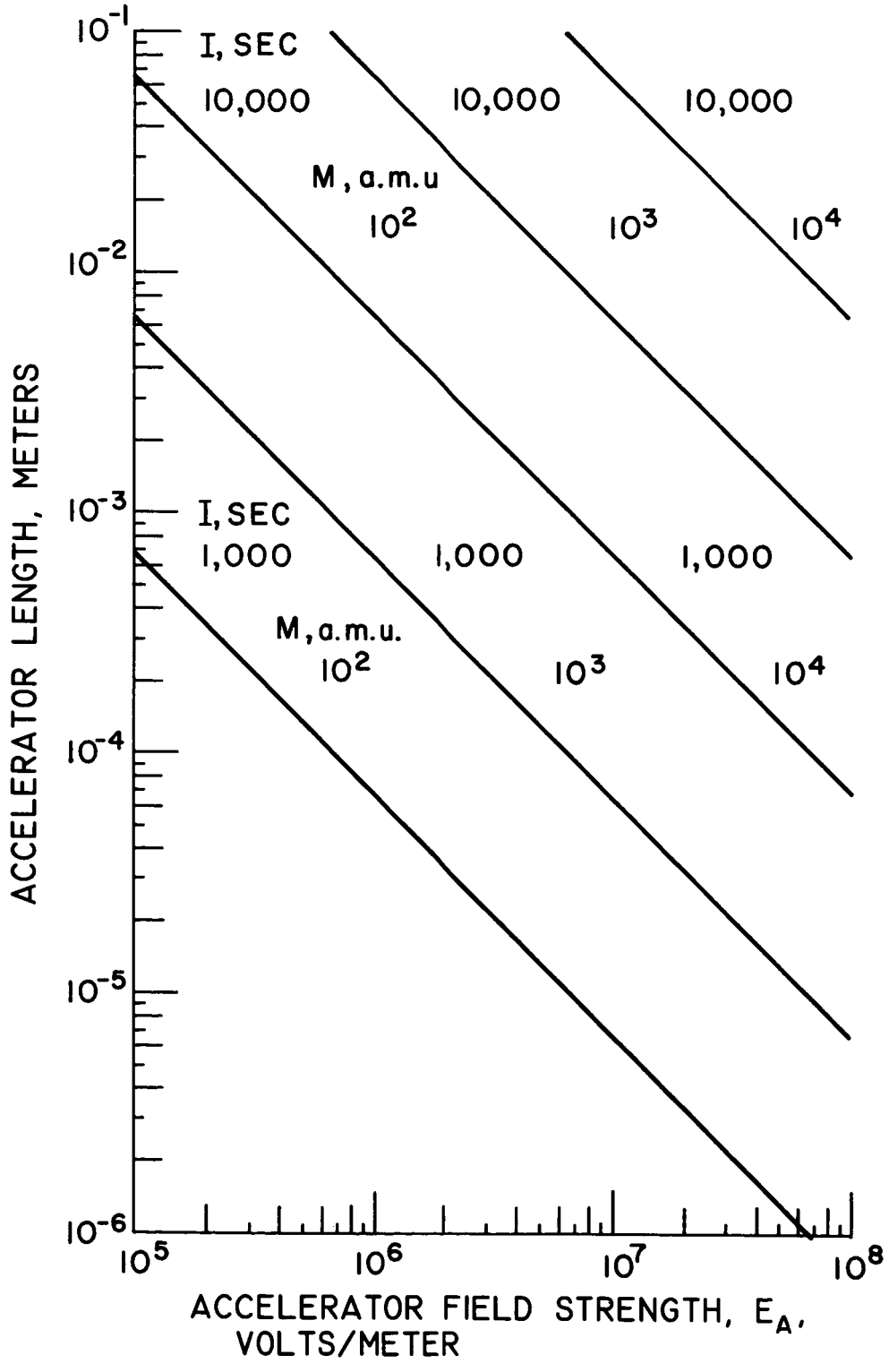

Figure 6. - Effect of accelerator electric field strength on accelerator length of Child's Law accelerators. $\Delta V_A/\Delta V_{net} = 1.0$, singly charged particles.

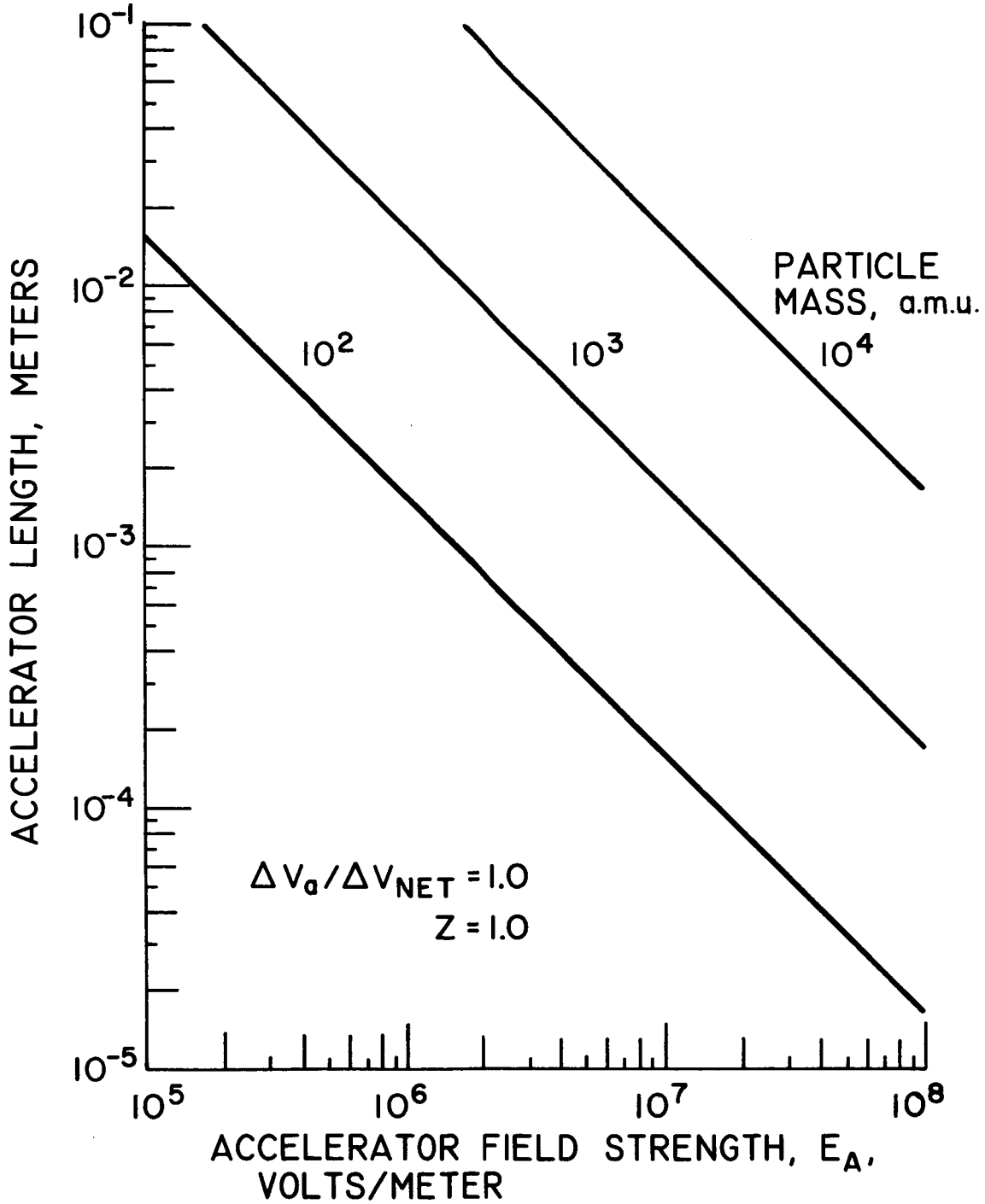

Figure 7. - Effect of accelerator electric field strength on Child's Law accelerator length at specific impulse of 5,000 seconds.

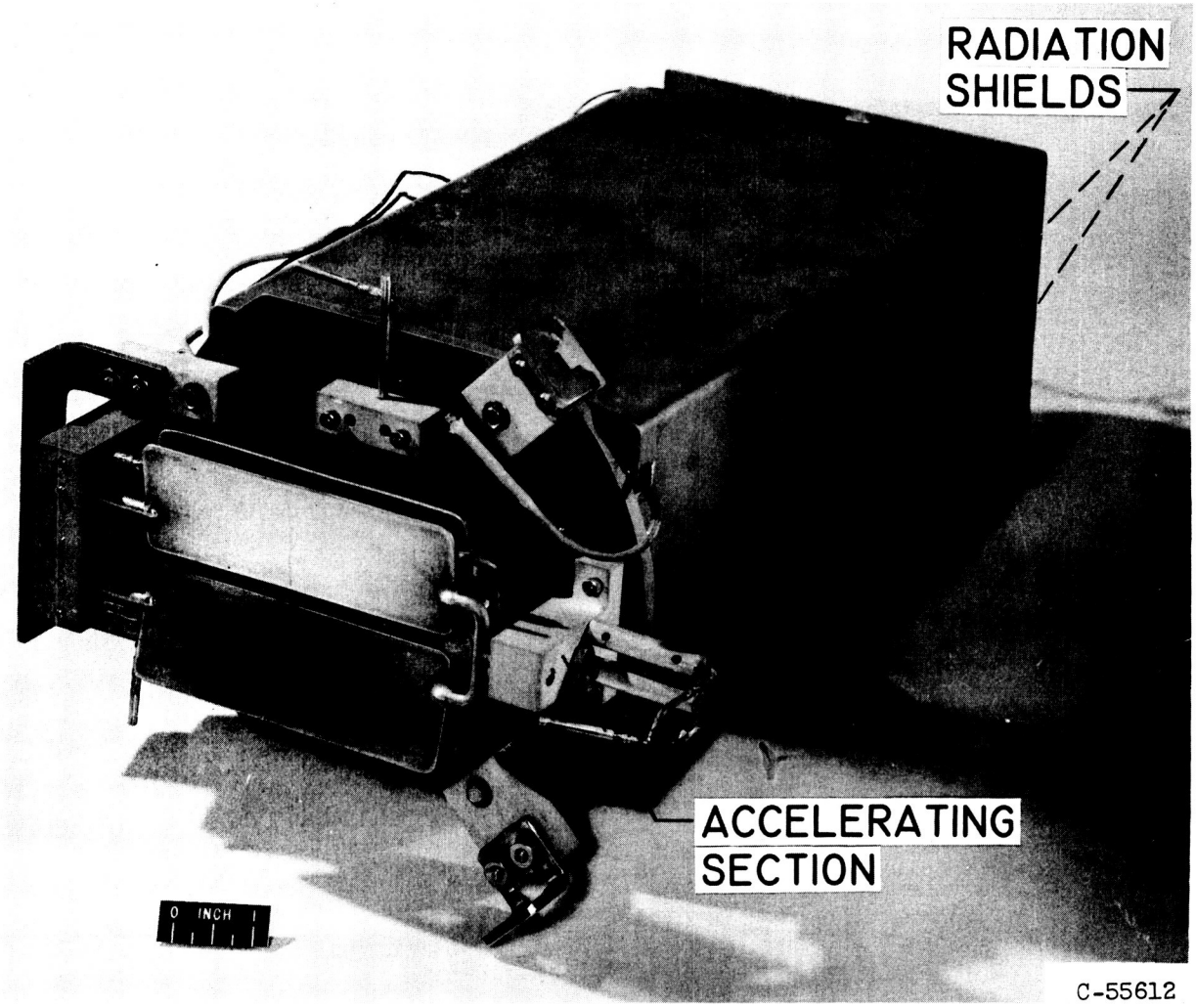

(a) General configuration.

Figure 8. - Colloidal-particle electrostatic engine.

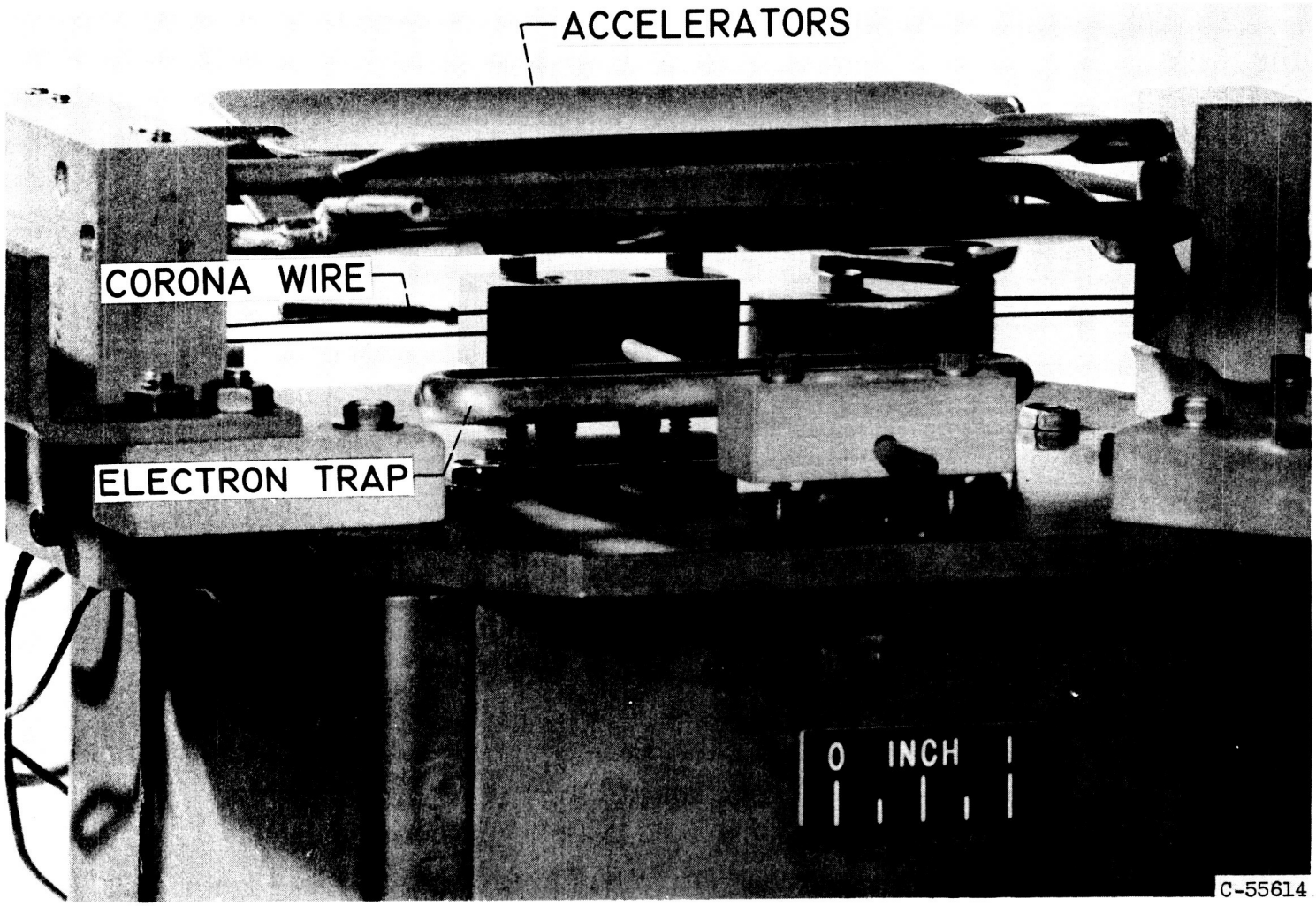

(b) Detail of accelerators showing corona wire and ring electron trap.

Figure 8. - Continued. Colloidal-particle electrostatic engine.

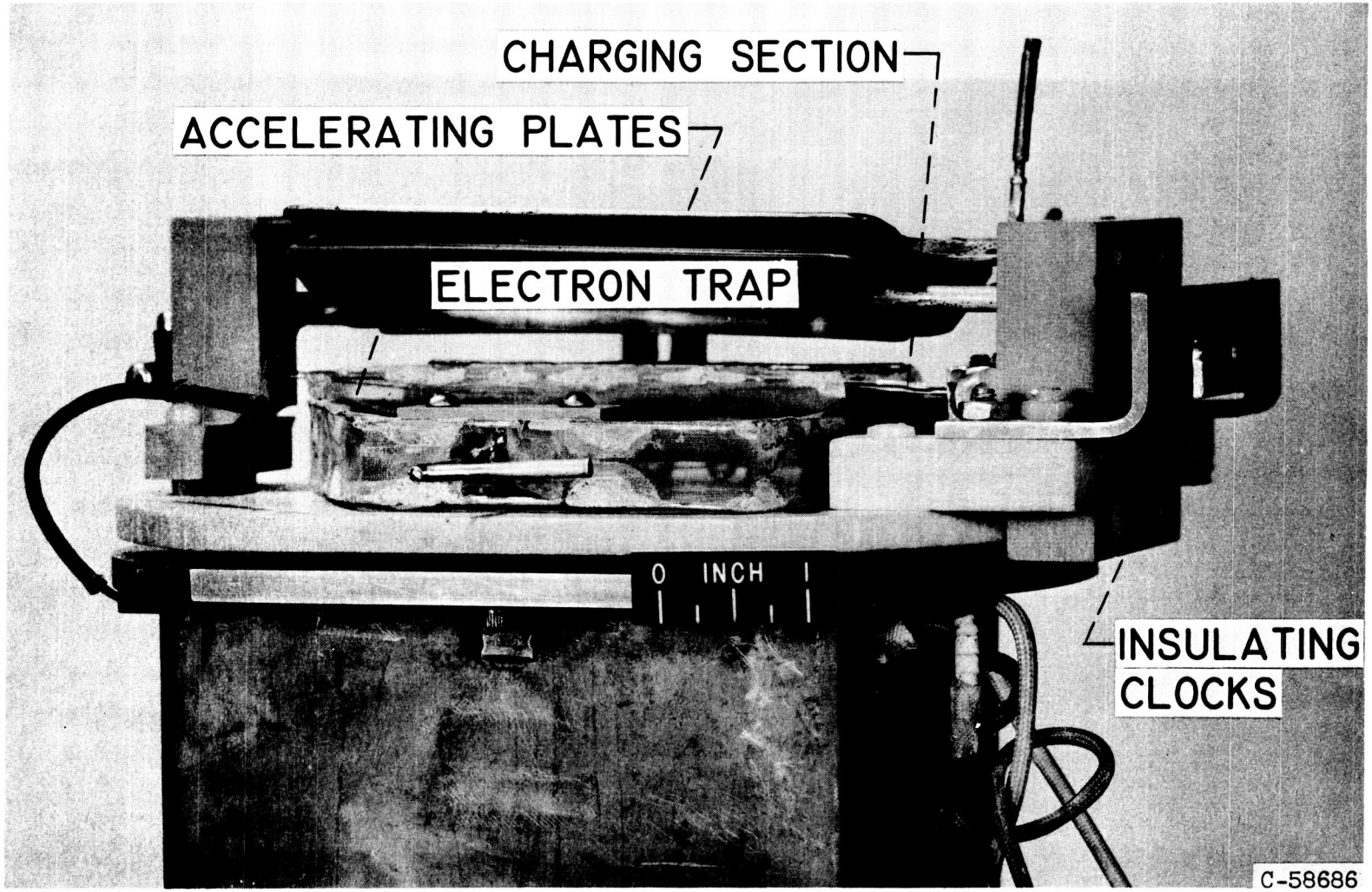

(c) Detail of accelerating section.

Figure 8. - Concluded. Colloidal-particle electrostatic engine.

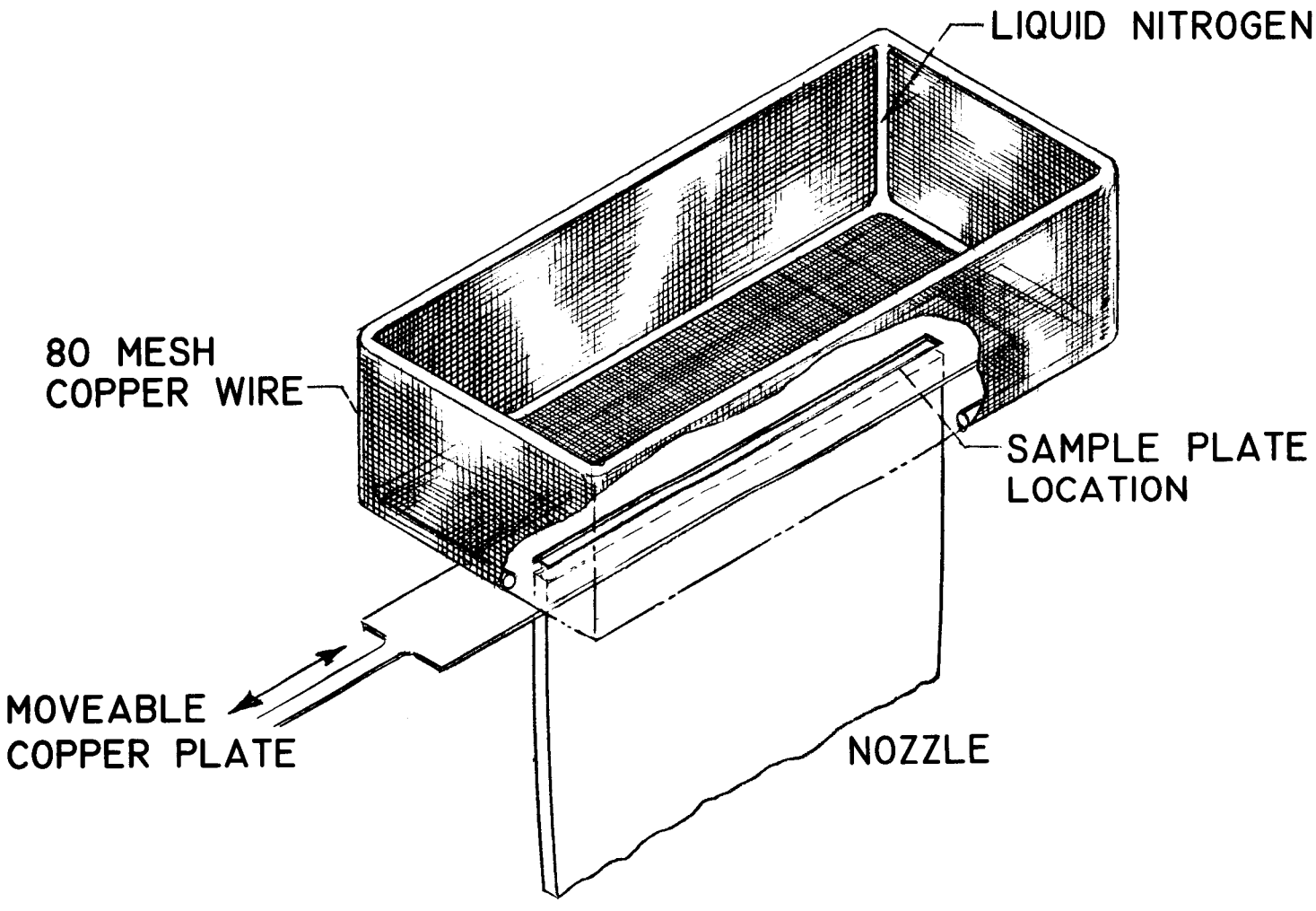

(a) Collection technique.

Figure 9. - Sample collection at exit of colloidal-particle generator.

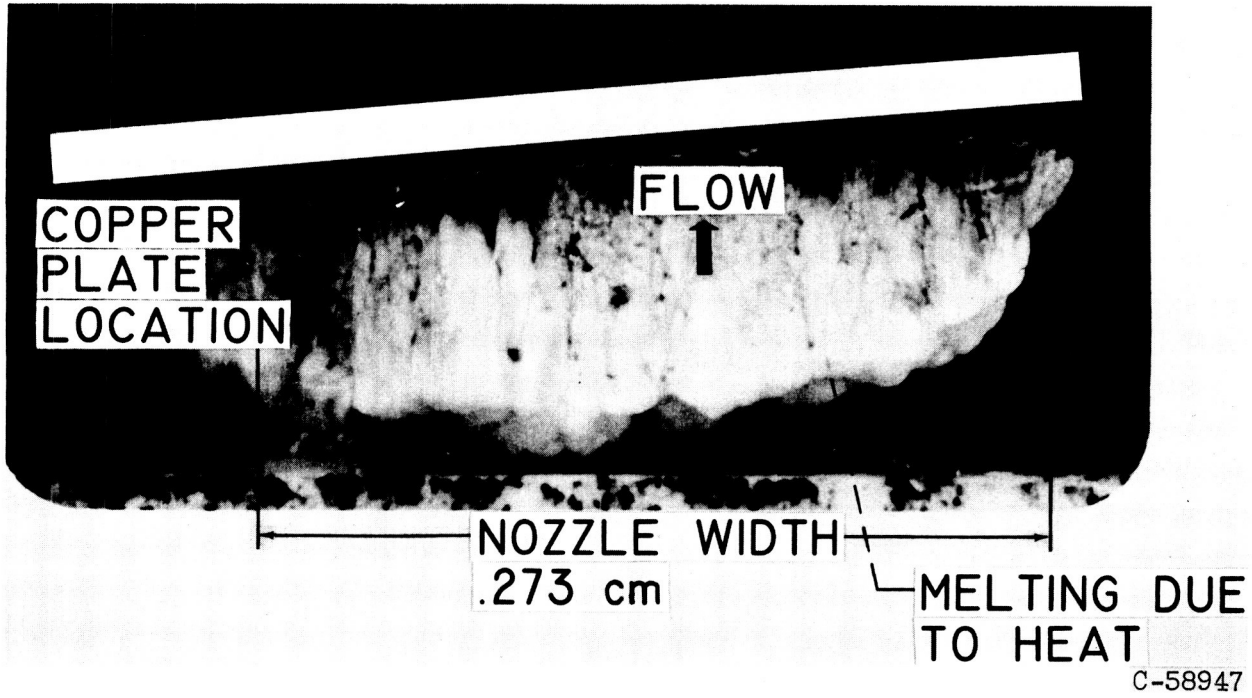

(b) Cross-section.

Figure 9. - Concluded. Sample collection at exit of colloidal-particle generator.

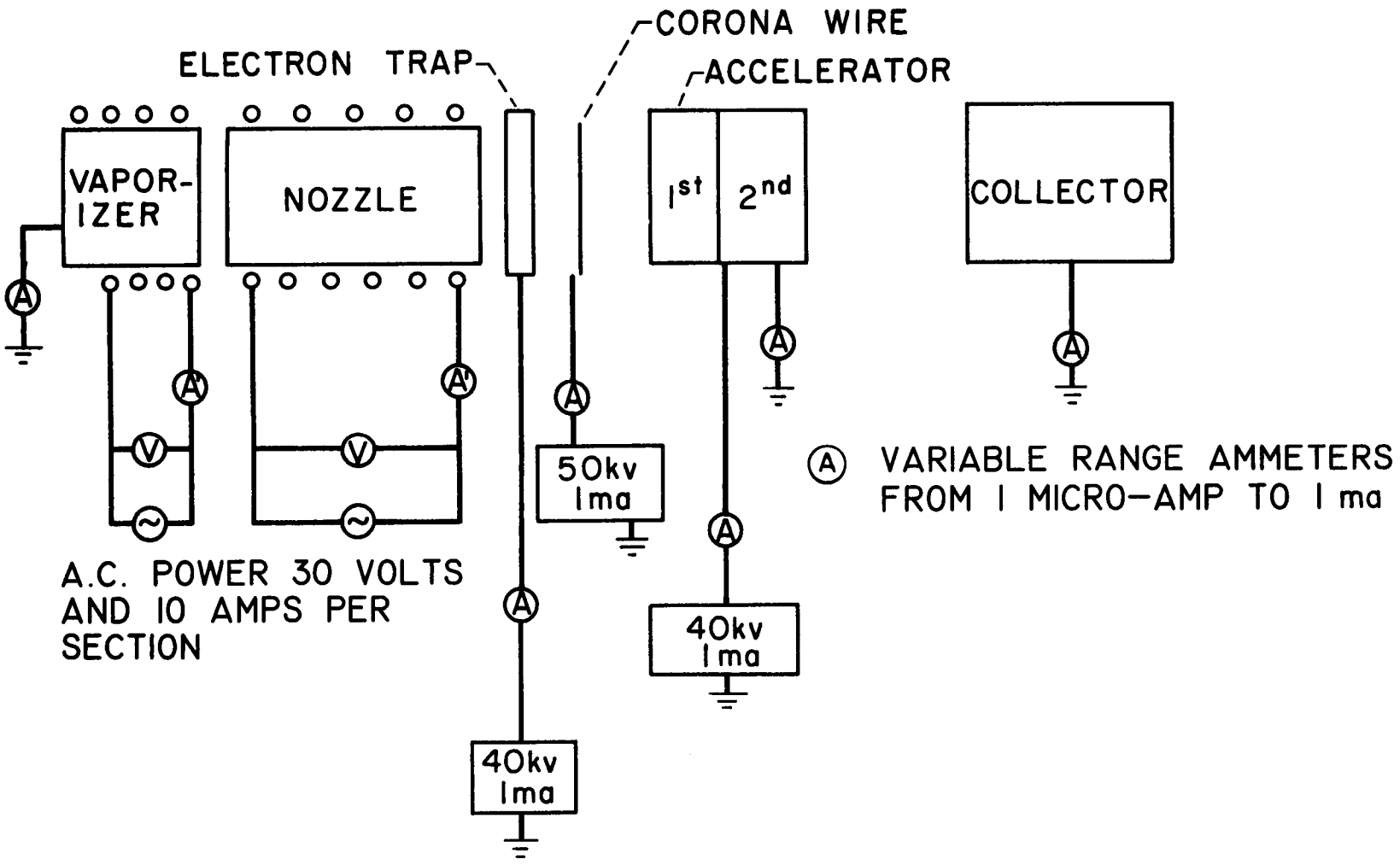

Figure 10. - Power supply and metering system as used with the colloidal engine.

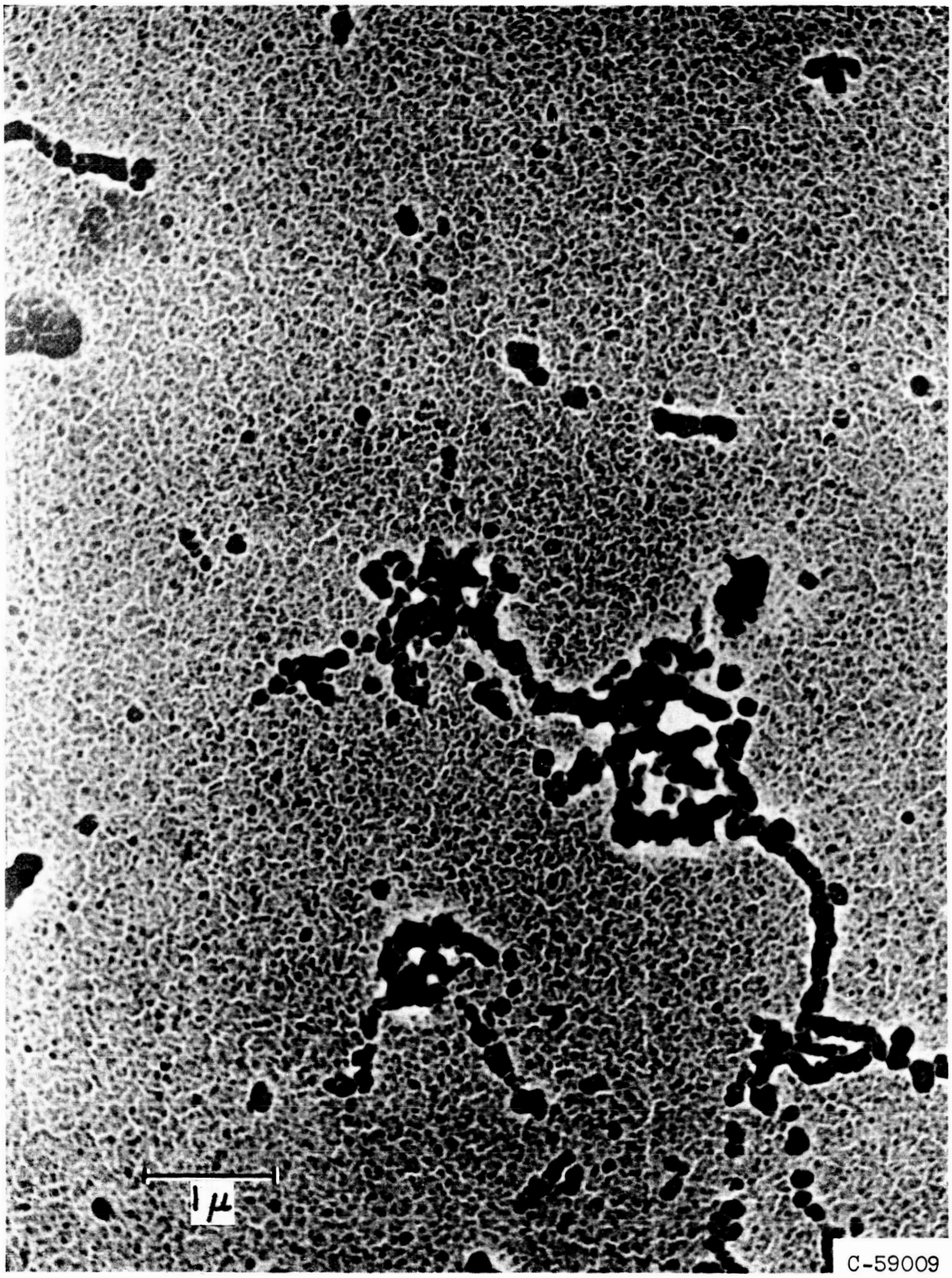

(a) Operating temperature, 400° K.

Figure 11. - Particle size of mercuric chloride.

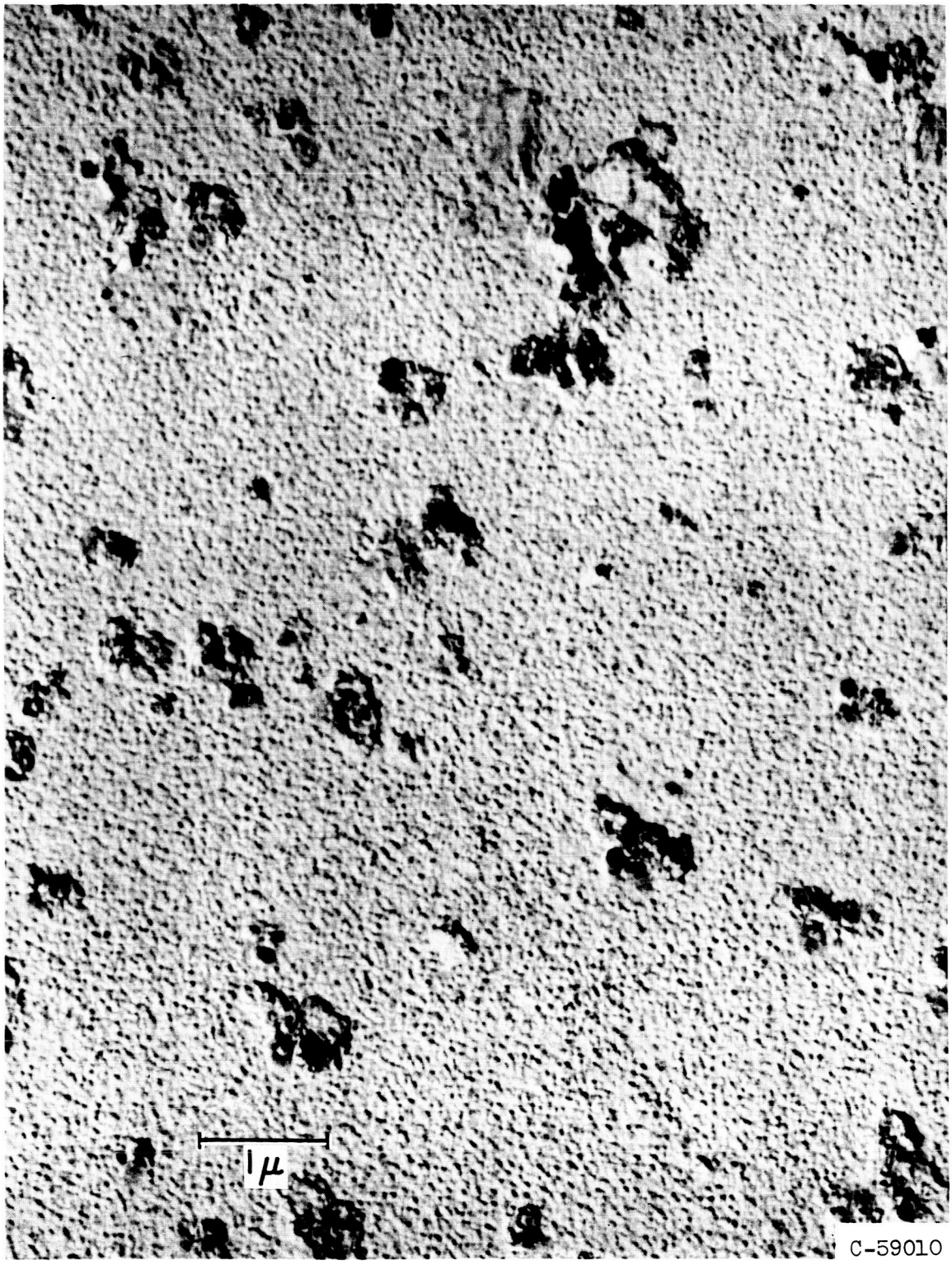

(b) Operating temperature, 430° K.

Figure 11. - Concluded. Particle size of mercuric chloride.

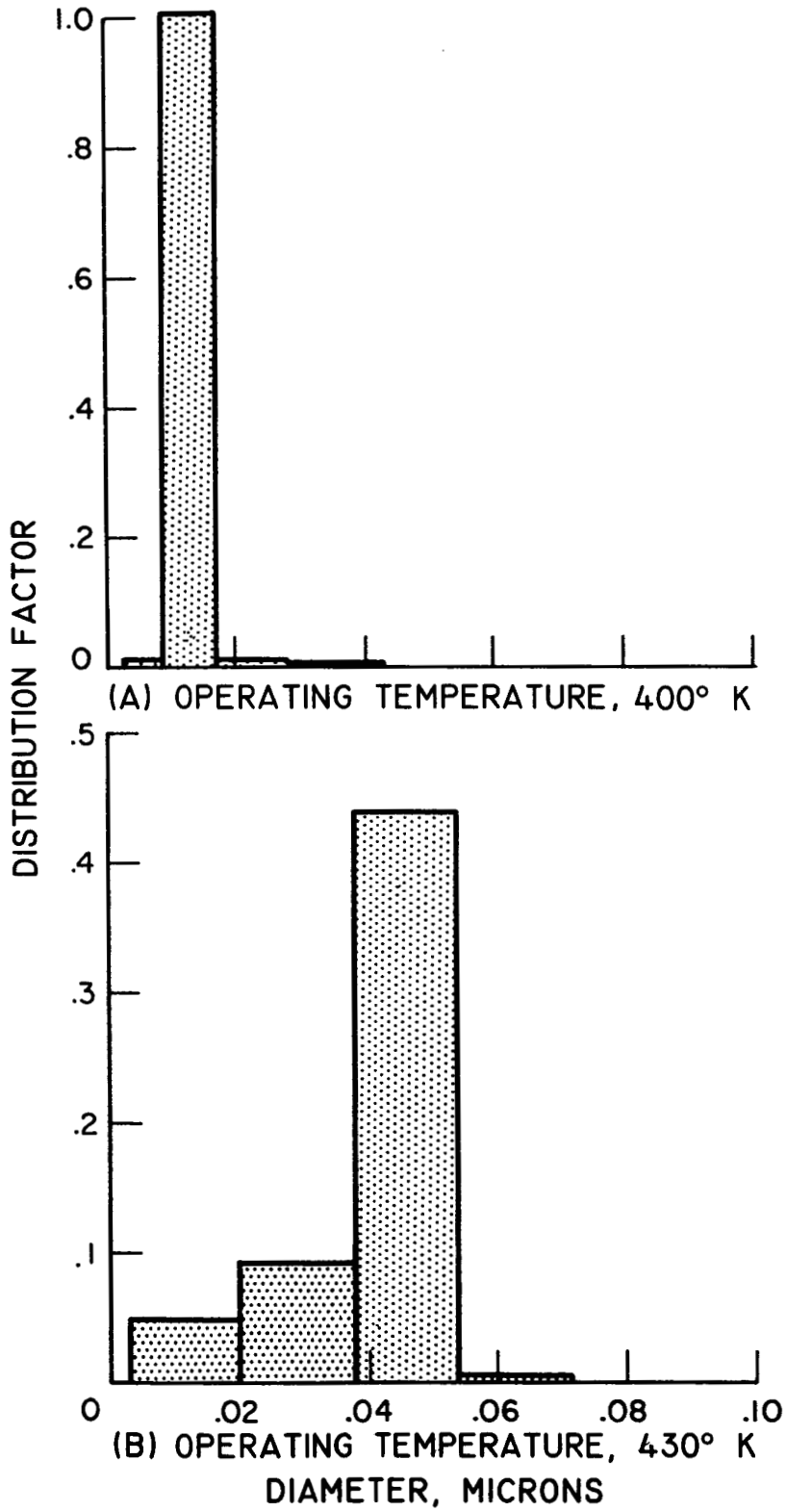

Figure 12. - Particle distribution of mercuric choloride.

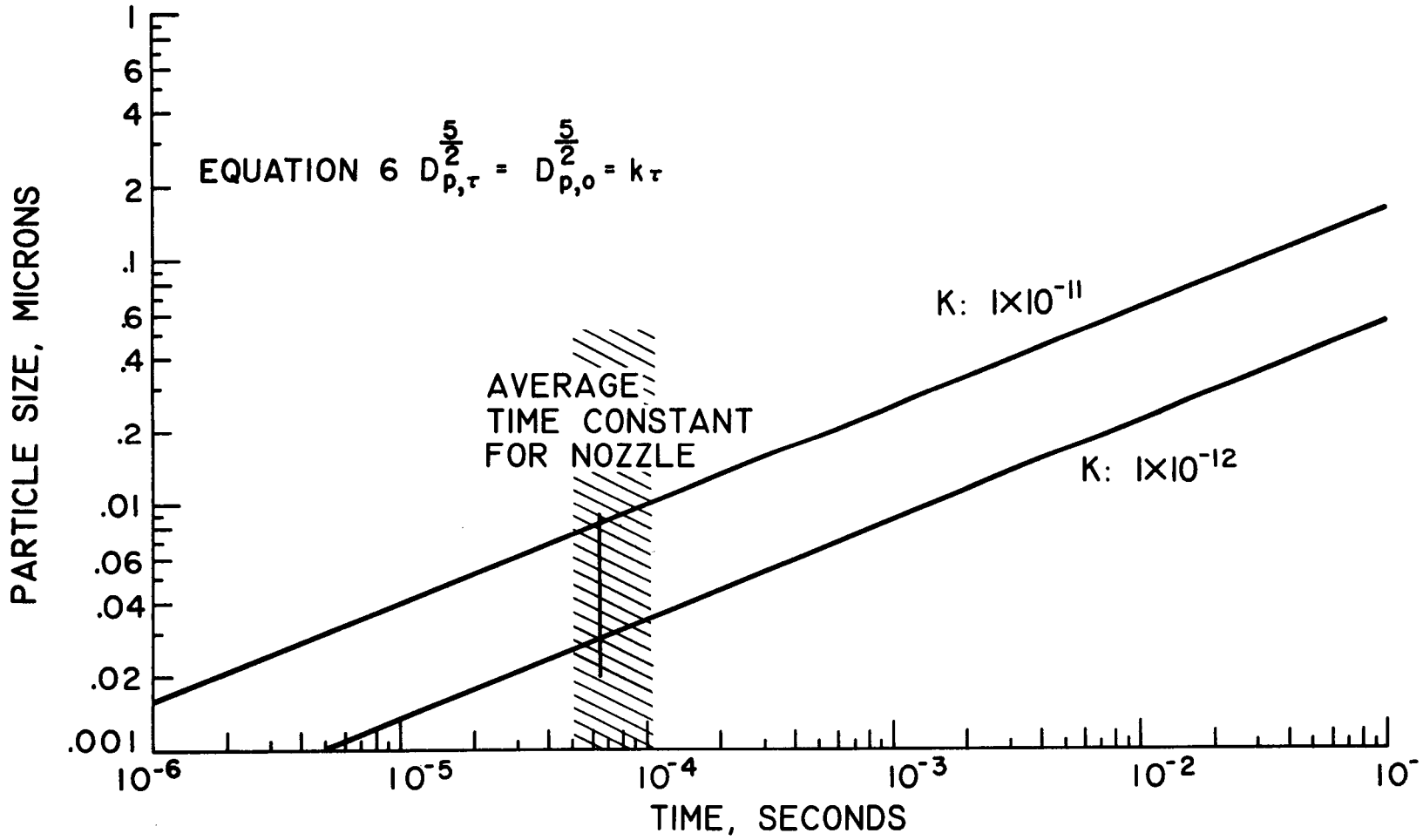

Figure 13. - Comparison of actual particle size to predicted particle size.

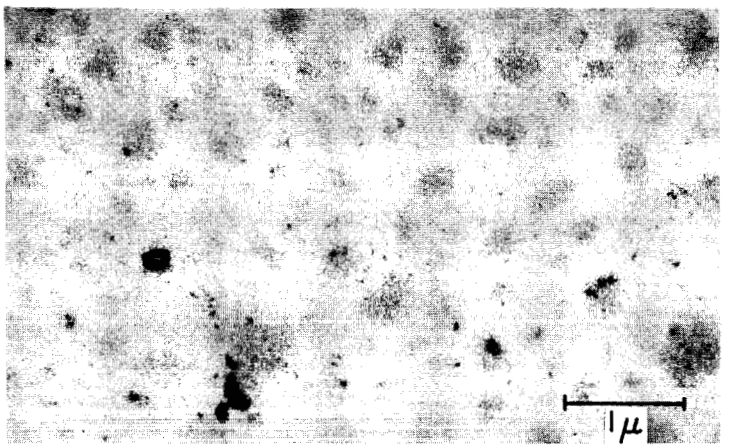

(a) Particle size.

C-59008

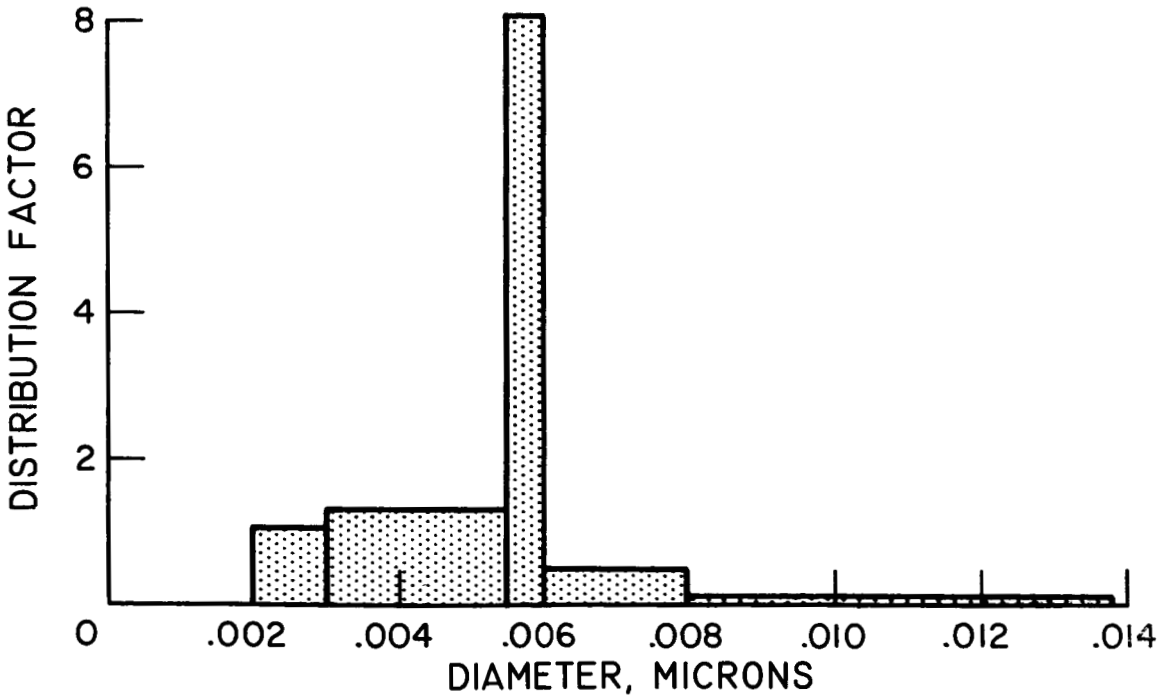

(b) Particle distribution of aluminum chloride.

Figure 14. - Particle size of aluminum chloride.

(a) Run 1.

Figure 15. - Particle size of mercurous chloride.

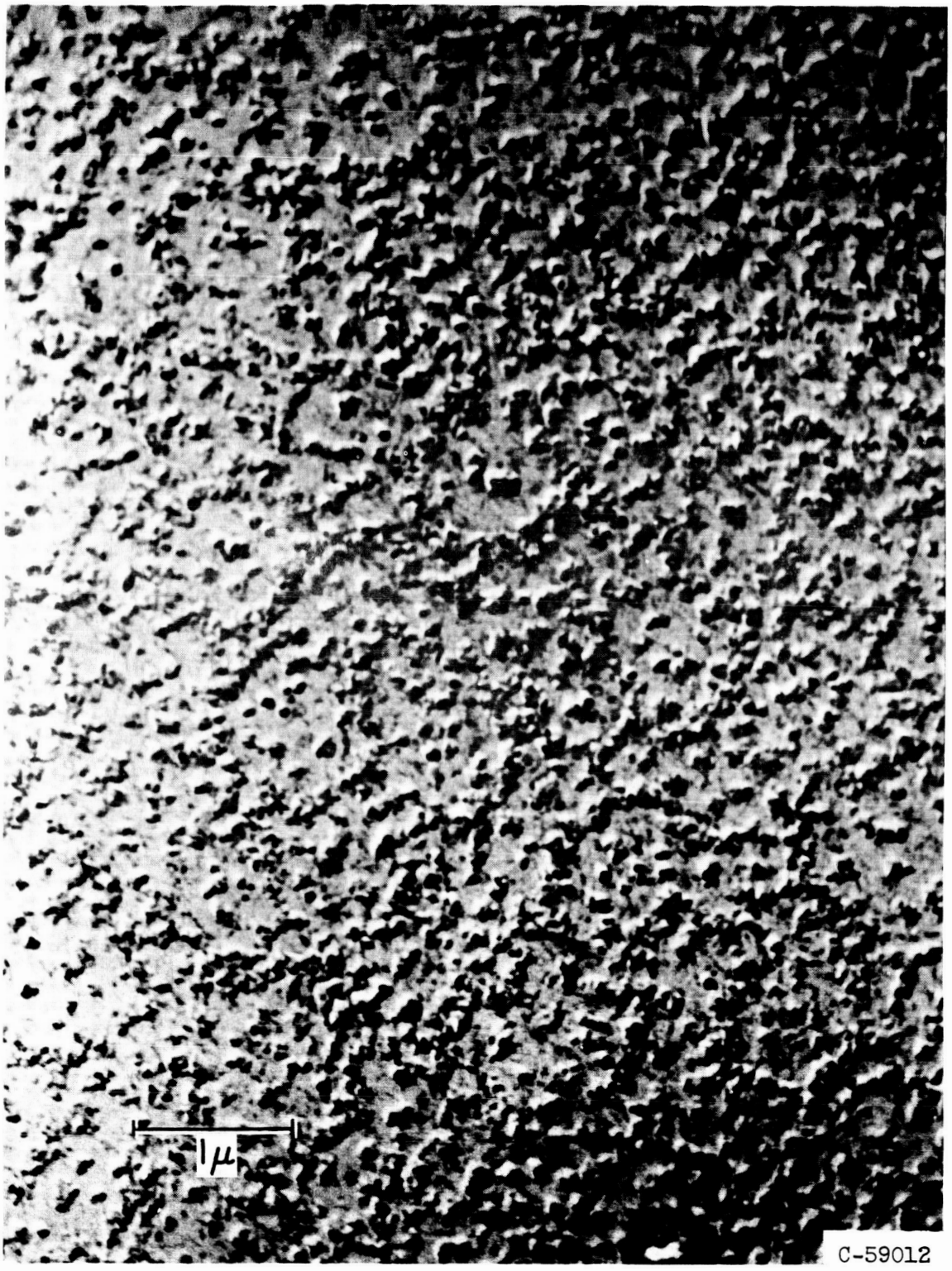

(b) Run 2.

Figure 15. - Concluded. Particle size of mercurous chloride.

E-1578

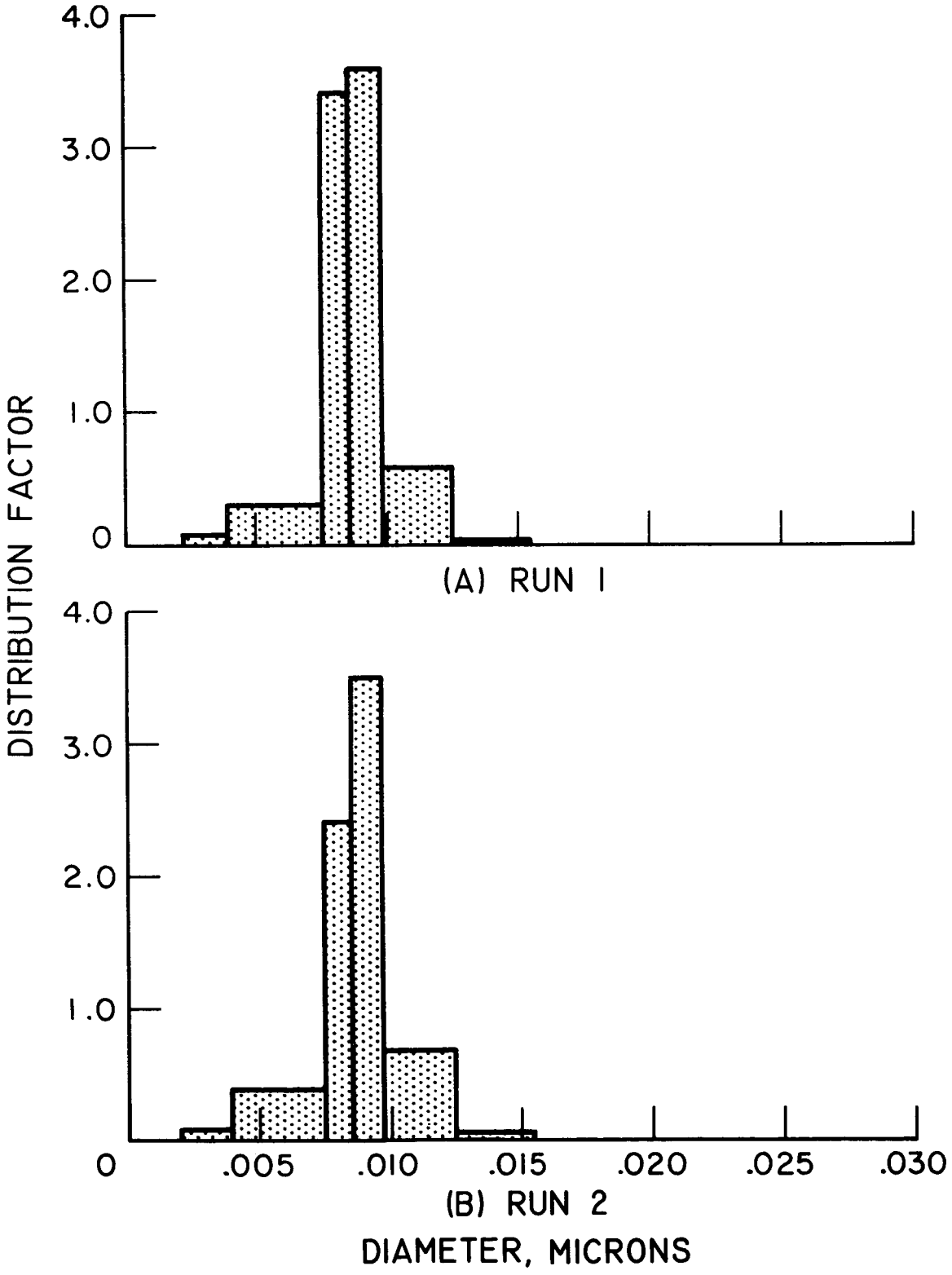

Figure 16. - Particle distribution of mercurous chloride.

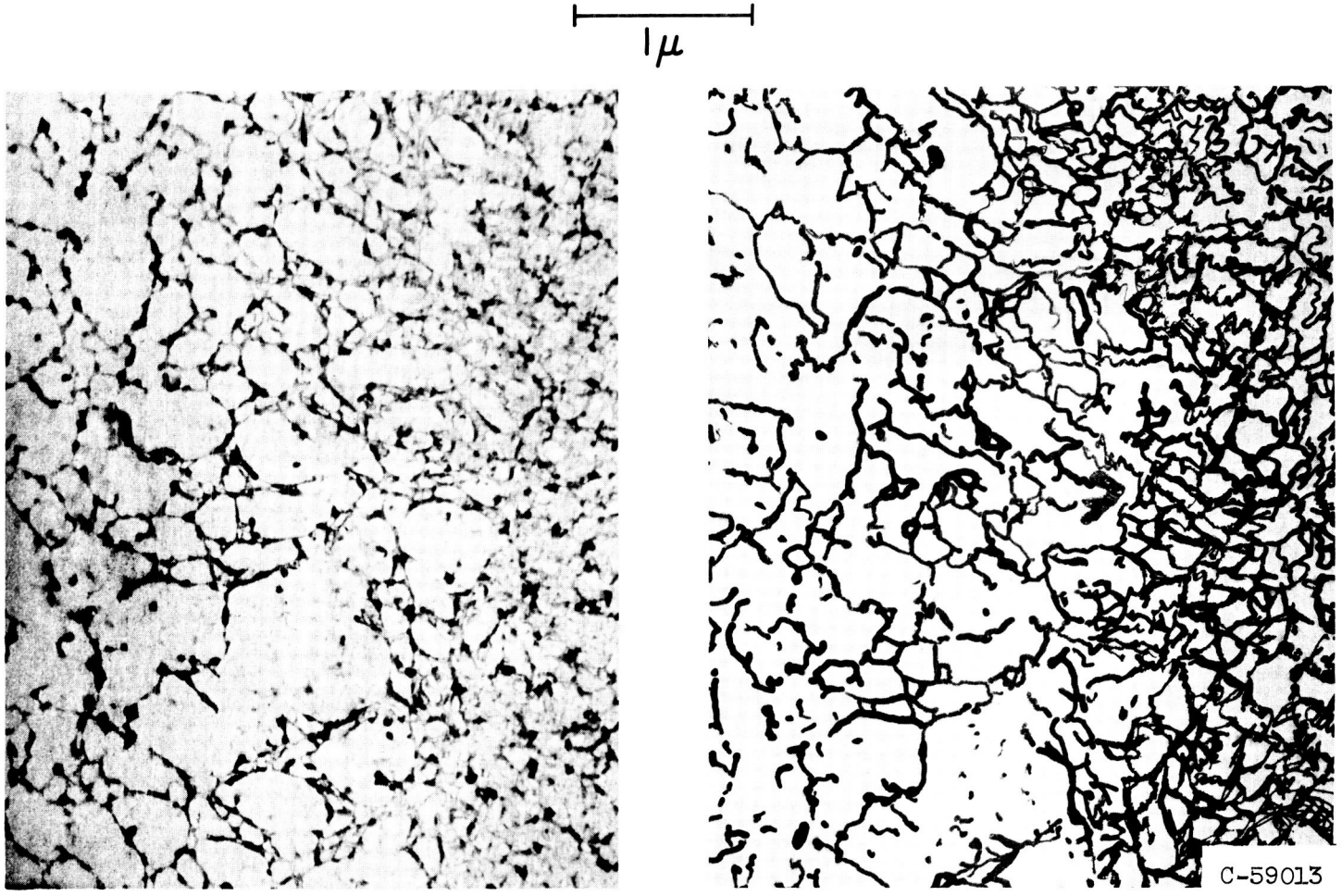

(a) Original photograph.

(b) Opaqued photograph.

Figure 17. - Partial deposit of mercurous chloride.

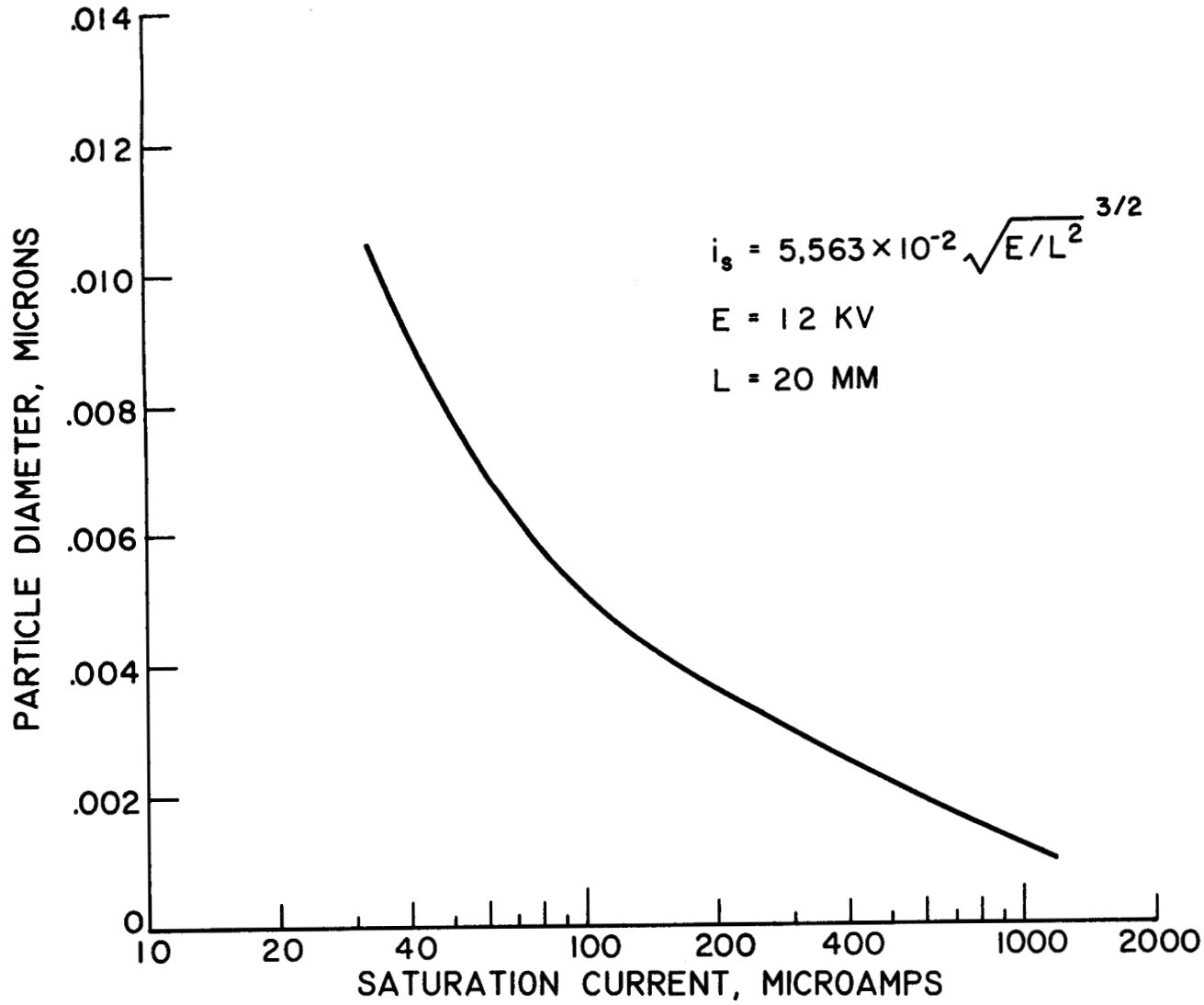

Figure 18. - Space charge limited flow for the colloidal particle electrostatic engine.

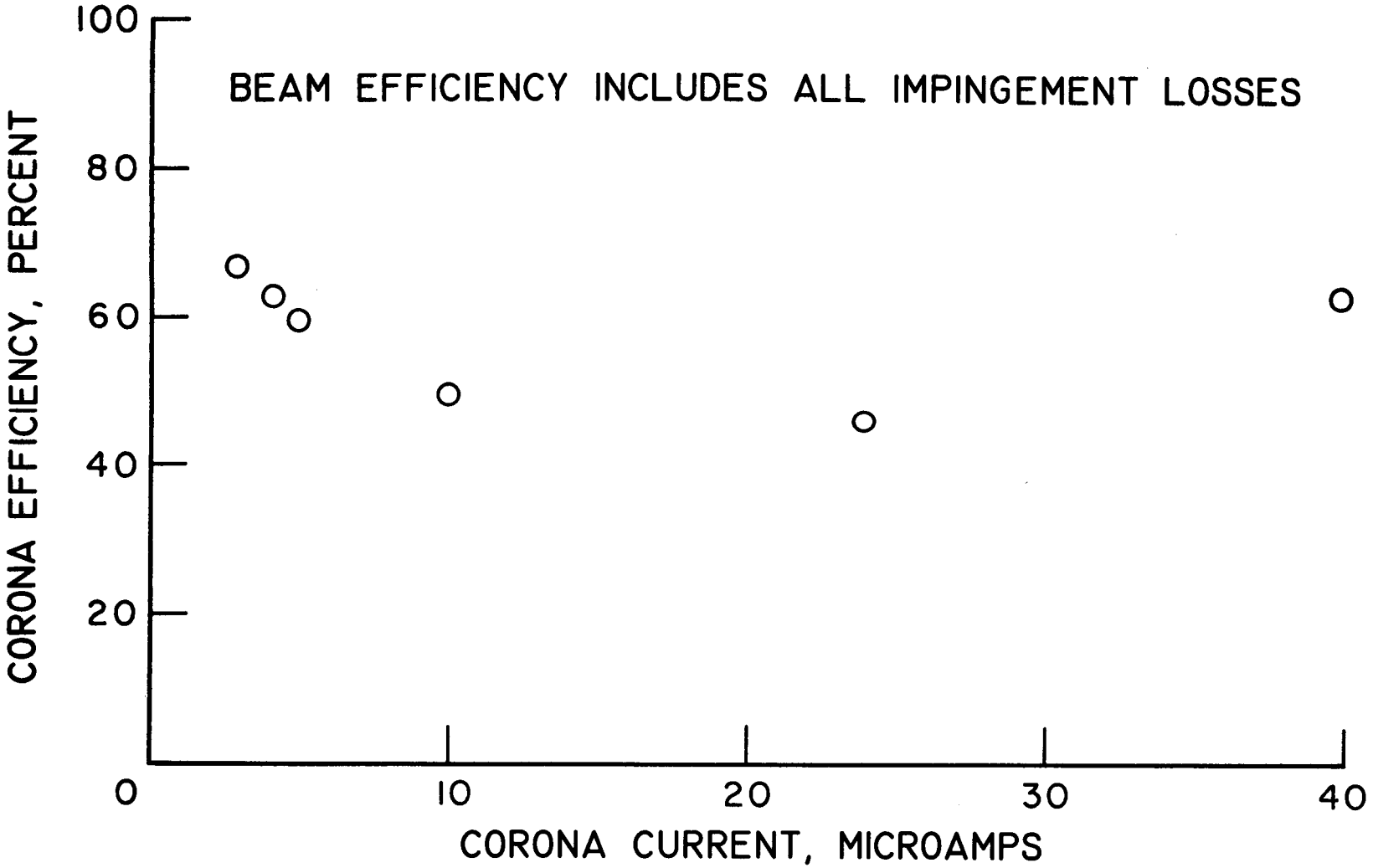

Figure 19. - Beam efficiency of colloidal-particle electrostatic engine.

NASA-CLEVELAND, OHIO E-1578